Numerical Analysis on 3D Microfluidic Paper Based Analytical Device

Author

Zeeshan Abid

Registration Number

00000274182

Supervisor

Dr. Zaib Ali

DEPARTMENT OF MECHANICAL ENGINEERING

SCHOOL OF MECHANICAL & MANUFACTURING ENGINEERING

NATIONAL UNIVERSITY OF SCIENCES AND TECHNOLOGY

ISLAMABAD

August, 2022

Numerical Analysis on 3D Microfluidic Paper Based Analytical Device

Author

Zeeshan Abid

Registration Number

00000274182

A thesis submitted in partial fulfillment of the requirements for the degree of

MS Mechanical Engineering

Thesis Supervisor:

Dr. Zaib Ali

Thesis Supervisor's Signature: _____

DEPARTMENT OF MECHANICAL ENGINEERING

SCHOOL OF MECHANICAL & MANUFACTURING ENGINEERING

NATIONAL UNIVERSITY OF SCIENCES AND TECHNOLOGY,

ISLAMABAD

August, 2022

THESIS ACCEPTANCE CERTIFICATE

Certified that final copy of MS thesis written by Mr. **Zeeshan Abid** Registration No. **00000274182** of **SMME** has been vetted by undersigned, found complete in all aspects as per NUST Statutes/Regulations, is free of plagiarism, errors, and mistakes and is accepted as partial fulfillment for award of MS/MPhil degree. It is further certified that necessary amendments as pointed out by GEC members of the scholar have also been incorporated in the said thesis.

Signature with stamp: _____

Name of Supervisor: **Dr. Zaib Ali**

Date: _____

Signature of HoD with stamp: _____

Date: _____

Countersign by

Signature (Dean/Principal): _____

Date: _____

Declaration

I certify that this research work titled "*Numerical Analysis on 3D Microfluidic Paper Based Analytical Device"* is my own work. The work has not been presented elsewhere for assessment. The material that has been used from other sources has been properly acknowledged / referred.

Signature of Student

Zeeshan Abid

2022-NUST-MS-Mech-00000274182

Plagiarism Certificate (Turnitin Report)

This thesis has been checked for Plagiarism. Turnitin report endorsed by Supervisor is attached.

Signature of Student

Zeeshan Abid

Registration Number

00000274182

Signature of Supervisor

Copyright Statement

- Copyright in text of this thesis rests with the student author. Copies (by any process) either in full, or of extracts, may be made only in accordance with instructions given by the author and lodged in the Library of NUST School of Mechanical & Manufacturing Engineering (SMME). Details may be obtained by the Librarian. This page must form part of any such copies made. Further copies (by any process) may not be made without the permission (in writing) of the author.
- The ownership of any intellectual property rights which may be described in this thesis is vested in NUST School of Mechanical & Manufacturing Engineering, subject to any prior agreement to the contrary, and may not be made available for use by third parties without the written permission of the SMME, which will prescribe the terms and conditions of any such agreement.
- Further information on the conditions under which disclosures and exploitation may take place is available from the Library of NUST School of Mechanical & Manufacturing Engineering, Islamabad.

Acknowledgements

First and foremost, I am thankful to my Creator Allah Subhana-Watala to have guided me throughout this work at every step and for every new thought which You setup in my mind to improve it. Indeed, I could have done nothing without Your priceless help and guidance. Whosoever helped me throughout the course of my thesis, whether my parents or any other individual was Your will, so indeed none be worthy of praise but You.

I am profusely thankful to my supervisor Dr. Zaib Ali for his help throughout my thesis. I found his office door always open whenever I need his assistance. I really appreciate his kindness, patience and guidance throughout my whole thesis. I would also like to thank him for teaching me professionalism and research ethics.

I would also like to thank Dr. Emad Uddin, Dr. Muhammad Sajid, Dr. Jawad Aslam for being on my thesis guidance and evaluation committee. Their critical review of my work has always proved to be very valuable for me. I would also like to extend my gratitude to my colleagues: Muhammad Usman for his motivation and cooperation with the computational resources and Muhammad Rizwan for my thesis write up and presentation.

I would also like to offer my gratitude to my beloved Mother and Sister who continued to support me throughout in every department of my life. Finally, I would like to express my gratitude to all the individuals who have rendered valuable assistance to my study.

Dedicated to my Mother and teachers

Abstract

Paper-based microfluidics are microfluidic devices that consist of a series of hydrophilic cellulose or nitrocellulose fibers that transport fluid from an inlet through the porous medium to a desired outlet or region of the device, by means of capillary action. Paper is abundant and compatible with many chemical/biochemical/medical applications, it is easy to use, disposable, equipment free, and its high surface area improves detection limits for colorimetric method, its ability to store reagents in active form within the fiber network. It provides a novel system for fluid handling and fluid analysis for a variety of applications including health diagnostics, environmental monitoring as well as food testing. It has been used from spot tests for metals and paper chromatography to lateral flow immunoassays and later now as multilayered (µPADs). Different technologies has been adopted in past for fabrication of (µPADs). The fundamental principle underlying these fabrication techniques is to pattern hydrophilic-hydrophobic contrast on a sheet of paper in order to create micron-scale (i.e., hundreds to thousands of micrometers) capillary channels on paper. Their widespread adoption has been limited by slow flow rates of fluid passing through it, shelf life of enzyme/reagent stored on paper, coffee ring effect in which there is non-uniform distribution of reagent due to hydrophobic boundary, theoretical modeling which accurately depicts behavior of fluid flow through multilayered µPADs considering all design parameters, non-homogenous paper causes anisotropic properties. In counter to that in this present work, numerical analysis of impact of various design parameters on the performance of single and multilayered paper based microfluidic analytical devices (µPADs) is performed, in order to find effect of different design parameters on velocity of fluid e.g. porosity, permeability, capillary angle, gap height, surface tension, dynamic viscosity, paper thickness, paper width etc. Based on the results of numerical analysis, it is concluded that permeability, gap height, interfacial tension, paper thickness are directly proportional with the velocity of fluid and the remaining design parameters dynamic viscosity, capillary angle are inversely proportional with the velocity of fluid, porosity doesn't affect velocity value. Whatman filter paper grade 4 is recommended for single layered and multilayered microPADs, because velocity of fluid is found to be 1.3 mm/s in case of single layered microPADs. Maximum gap height that is beneficial for velocity enhancement in multilayered microPADs is 400 µm. Optimum value of paper width is found to be 0.02m for enhanced velocity. Based on these findings one can manufacture paper material of certain desired properties to get favorable results and can also fabricate multilayered microPADs while keeping gap height behavior under consideration.

Table of Contents

Declaration ii
Plagiarism Certificate (Turnitin Report) iii
Copyright Statement iv
Acknowledgements v
Abstract vii
Table of Contents viii
List of Figures x
Nomenclature and Symbols xii
1 : INTRODUCTION 1
2 : LITERATURE REVIEW 9
3 : METHODOLOGY 13
3.1 Multiphase Transport in Porous Media: 13
3.1.1 Darcy's Law interface: 14
3.1.2 Governing Equations of Phase Transport in Porous Media: 14
3.2 Governing Equations of Free and Porous Media Flow Interface: 15
4 : RESULTS AND DISCUSSION 18
4.1 Whatman filter paper grade 1: 18
4.2 Whatman filter paper grade 3: 20
4.3 Whatman Filter Paper Grade 4: 21
4.4 Whatman filter paper grade 5: 22
4.5 Solving ODEs obtained from Experiments performed on Multilayered µPADs using MATLAB Software: 25
4.5.1 Validation results: 25
4.5.2 Effect of interfacial tension: 27
4.5.3 Effect of fluid dynamic viscosity: 28
4.5.4 Effect of paper thickness: 30
4.5.5 Effect of fluid contact angle on paper: 31
4.5.6 Effect of gap height: 33
5 : CONCLUSION AND FUTURE RECOMMENDATIONS 34

REFRENCES..36

List of Figures

Figure 1.1: Schematic and Orientation of Multilayered (µPADs) [73] 1

Figure 1.2: (a) Side View Picture and (b) illustrative schematic of fluid flow in Multilayered (µPADs) (390 µm gap height) [73].....2

Figure 1.3: Filter Paper pores with 500 times under the scanning of electron microscope 2

Figure 1.4: Whatman filter paper available with different grades [56].....3

Figure 3.1: Parameters used for single and multilayered µPADs numerical analysis 17

Figure 3.2: Mesh of single layered µPADs 17

Figure 4.1: Parameters used for numerical analysis of single layered Whatman filter paper 18

Figure 4.2:Volume fraction plot of Whatman filter paper grade 1 18

Figure 4.4: Surface pressure, streamline Darcy's velocity field.....19

Figure 4.3: Water saturation in 3D 19

Figure 4.5: Volume fraction plot of Whatman filter paper grade 3 20

Figure 4.6: Parameters used for numerical analysis of single layered Whatman filter paper 20

Figure 4.7: Volume fraction plot of whatman filter paper grade 4 21

Figure 4.8: Parameters used for numerical analysis of single layered Whatman filter paper 21

Figure 4.9: Volume fraction plot of Whatman filter paper grade 5 22

Figure 4.10: Parameters used for numerical analysis of single layered Whatman filter paper grade 5.....22

Figure 4.11: Velocity VS Time graph for two different pore radius and at different porosity value from 0 to 0.9 23

Figure 4.12: Velocity VS Time graph for seven different pore radius and at constant porosity value of 0.5 23

Figure 4.13: Surface plot of Velocity magnitude 24

Figure 4.14: Whatman filter paper grade 4 properties used for numerical analysis of multilayered µPADs 25

Figure 4.15: Comparison of Experimental and Simulation results for gap height of 234 µm 25

Figure 4.16: Comparison of Experimental and Simulation results for gap height of 312 µm 26

Figure 4.17: Comparison of Experimental and Simulation results for gap height of 312 µm 26

Figure 4.18: Comparison of Experimental and Simulation results for gap height of 390 µm 26

Figure 4.19: Velocity VS Time for 312 µm gap height with 03 different interfacial tension values 27

Figure 4.20: Velocity VS Time for 234 µm gap height with 03 different interfacial tension values 27
Figure 4.21: Velocity VS Time for 390 µm gap height with 03 different interfacial tension values 28
Figure 4.22: Velocity VS Time for 234 µm gap height with 03 different dynamic viscosity values 28
Figure 4.23: Velocity VS Time for 312 µm gap height with 03 different dynamic viscosity values 29
Figure 4.24: Velocity VS Time for 390 µm gap height with 03 different dynamic viscosity values 29
Figure 4.25: Velocity VS Time for 234 µm gap height with 03 different paper thickness values 30
Figure 4.26: Velocity VS Time for 390 µm gap height with 03 different paper thickness values 30
Figure 4.27: Velocity VS Time for 312 µm gap height with 03 different paper thickness values 31
Figure 4.28: Velocity VS Time for 234 µm gap height with 03 different fluid contact angles on the paper 31
Figure 4.29: Velocity VS Time for 312 µm gap height with 03 different fluid contact angles on the paper 32
Figure 4.30: Velocity VS Time for 390 µm gap height with 03 different fluid contact angles on the paper 32
Figure 4.31: Velocity VS Time for 10 different gap heights 33

Nomenclature and Symbols

µPADs	Microfluidic Paper Based Analytical Device
por/E_p	Porosity
K	Permeability
u	Velocity
P_v	Viscous pressure
P_c	Capillary pressure
θ	Capillary angle
γ	Interfacial surface tension
h	Half gap height
µ	Dynamic viscosity
t	Time
r	Pore radius
L	Penetration length of fluid
Q	Volumetric flow rate
A	Surface Area
ΔP	Pressure difference
q	Volumetric evaporation flux
t_h	Paper thickness
∇	Dell operator
ρ	Density
s	Different phases (s_1,s_2)
g	Gravitational acceleration
F	Body force

1 : INTRODUCTION

The main objective of this thesis is numerical analysis of impact of various design parameters e.g. porosity, pore radius, permeability, gap height, capillary angle, dynamic viscosity, paper thickness, surface tension, paper width etc. on the performance of single and multilayered paper based microfluidic analytical devices (µPADs), in order to get enhancement in velocity. This work is divided into three different portions:- (1) Numerical analysis of impact of various design parameters on single layered paper based microfluidic analytical device (µPADs) using COMSOL Multiphysics Software. (2) Numerical analysis of impact of various design parameters on multilayered paper based microfluidic analytical device (µPADs) using COMSOL Multiphysics Software. (3) Simulation of ODEs obtained from experimental work done by Robert B. Channon [73] using MATLAB Software. Below figures 1 & 2 are taken from Robert B. Channon Paper et al. [73] and this represents how multilayered microfluidic paper based devices are fabricated.

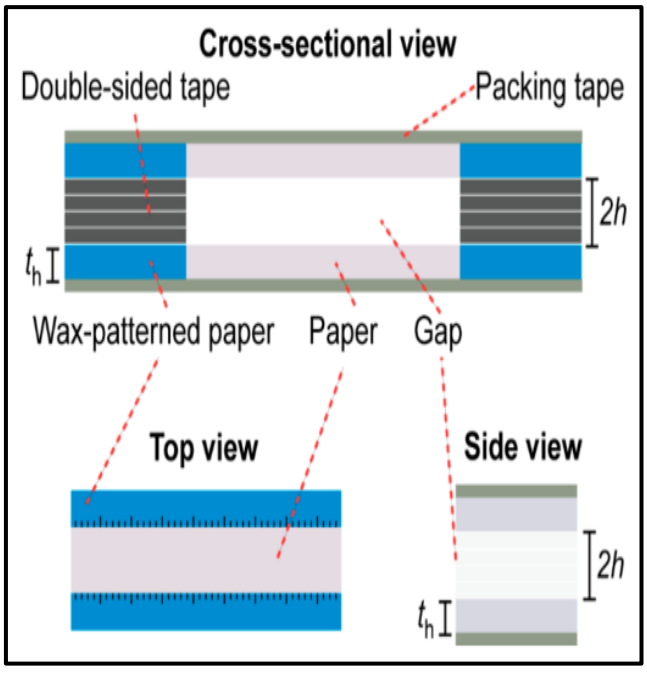

Figure 1.1: Schematic and Orientation of Multilayered (µPADs) [73]

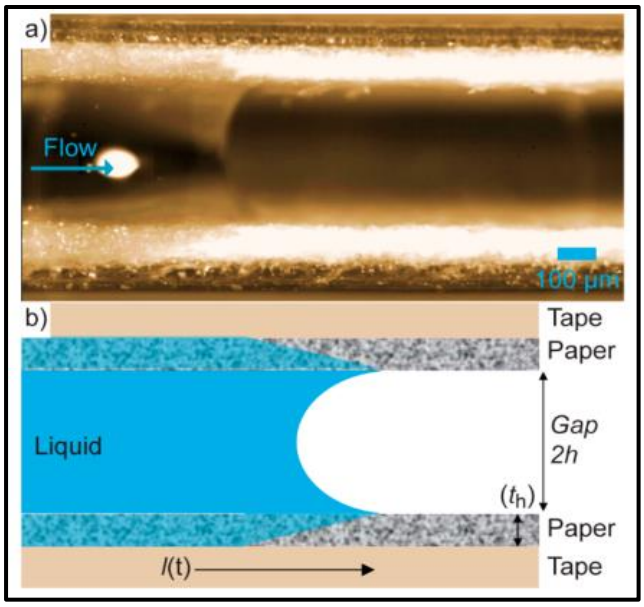

Figure 1.2: (a) Side View Picture and (b) illustrative schematic of fluid flow in Multilayered (µPADs) (390 µm gap height) [73]

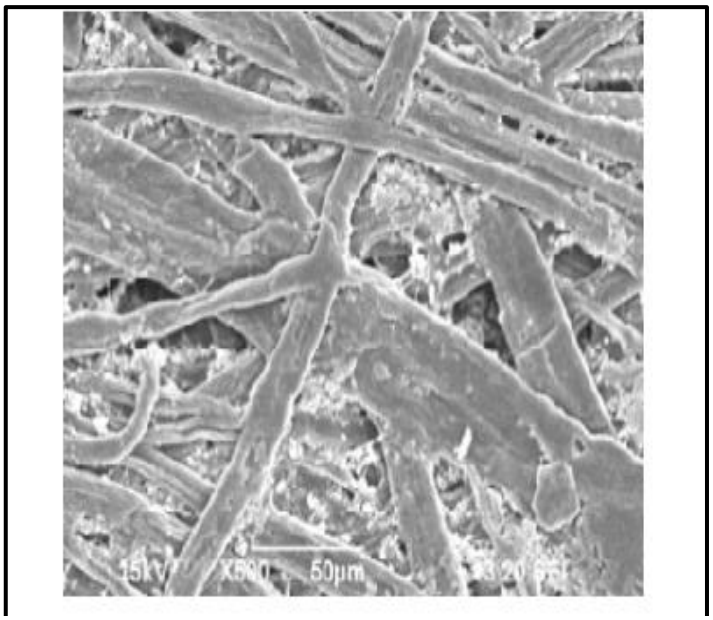

Figure 1.3: Filter Paper pores with 500 times under the scanning of electron microscope

Above figure is used to represent cylindrical pores of filter paper with micrometer radii and that's why paper behaves as a capillary device because these cylindrical pores helps to exhibit capillary phenomenon.

Figure 1.4: Whatman filter paper available with different grades [56]

Above figure represents whatman filter paper and it comes in different grades and possess different properties and are used in our case as filter paper for single layered and multilayered device.

As a substrate material for microfluidic assays, paper has been ignored until 2007, but after that Martinez et al. [6] reported the first microfluidic paper based analytical device (µPADs) for chemical analysis. The differentiative aspect of this work is that, hydrophobic (photoresist) patterning reagent is used to outline hydrophilic flow channels for giving direction to sample to move from an inlet to a defined location for multiple different analysis. Conventionally paper is defined as a flexible sheet made from an interlaced network of pressed cellulose fibers, but in the perspective of paper based microfluidics, it is defined as any porous membrane that wicks fluids by capillary action.

For making (Point of Care) POC diagnostic devices, paper has several unique advantages. It is inexpensive, abundant, and well-suited with a wide range of printing and processing techniques.

It can easily be laminated, transported and stored, and an entire industry already exists for large scale production of paper products, which could be given another dimension to produce paper based devices. Paper can be manufactured with different thicknesses and porosities. High densities of organic functional groups are presents on its surface area, which can be manipulated chemically to covalently or non-covalently bind reagents or analytes. It has a large surface to volume ratio, so advantage taken from this is as reagents and samples can be dried and stored on paper for later analysis, and this can be done using high speed printing techniques. It is best suited for colorimetric tests because of its inherited white background. It has different filtration and chromatographic properties, and can be used to separate analytes from complex samples such as blood and urine. Last but not least it wicks fluids by capillary action, so a paper based device can move fluids and perform an assay without any pumps or external sources of power. It is mostly described using the Lucas Washburn equation, which states that the length of flow is proportional to the square root of time. In the past most commonly used POC diagnostic technologies were dipstick assays and lateral flow assays (LFAs), however later µPADs build off dipstick and LFA technology and aimed to overcome the limitations of these two diagnostic platforms by enabling quantitative, sensitive, specific and multiplexed assays that are inexpensive and easy to use. Two steps were involved in fabrication of paper based µPADs: i) patterning paper, and ii) customizing the devices for their proposed applications, including applying reagents to the devices for assays. Steps before implementing patterning techniques includes computer generated design of the device. The design of the device will be determined by keeping in view its intended application and its patterning method. Any CAD software can be used to design a device (e.g., AutoCAD, Clewin, CorelDRAW, Illustrator, etc.). A free application was also developed specifically for designing µPADs called AutoPAD. The principle objective behind every technique for patterning paper is to create well defined patterns of hydrophobic barriers on a piece of paper to define hydrophilic channels and zones. Many different techniques for patterning paper have been developed including wax printing, photolithography, etching, cutting embossing, and inkjet printing. These techniques can be categorized into two types: i) physical patterning of paper by cutting, and ii) chemical patterning of paper with hydrophobic inks to create hydrophobic barriers. Each fabrication technique offers different advantages and disadvantages in terms of resolution of the patterns, fabrication time, chemical compatibility of the barriers, and requirements for equipment and reagents. Theoretical

aspects of transport in paper devices focused on elementary imbibition theory. Paper material choice is entirely dedicated on user application but can and will have significant and predictable impact on performance and fluidic transport consideration of substrate-analyte chemistry, wicking rate, material durability and fabrication methods. The most important characteristic of paper based microfluidic devices is their ability to wick fluids by capillary action; therefore, methods for controlling capillary wicking in paper based channels are essential to the field. Paper capillary wicking phenomenon has been studied and modeled extensively, and several different equations describing capillary wicking in paper have been published, with most involving some modifications of the Lucas Washburn equation. The simplest approach for controlling capillary wicking is by selecting the type of paper (pore size and porosity) and controlling the dimensions of the channels. Wicking can also be controlled by adding sugars to the paper based channels in high concentrations to slow capillary wicking. Enclosing paper based channels can influence capillary wicking by limiting evaporation. Stacking layers of paper, cutting a thin slit along the length of a paper based channel, or placing a plastic film on top of a paper based channel have also been shown to be useful mechanisms for increasing the rate of capillary wicking in paper based devices. Wicking based flow in capillary systems is considered laminar because fiber length scale and associated pores are typically less than 20 µm, resulting in low Reynolds numbers flow, hence classical flow dynamic behavior as long as effects of the fluid front can be ignored. Spontaneous imbibition in porous media with constant cross section, and with respect to short time scales, can be modeled by Darcy Law [18]: $Q = \frac{KA}{\mu L}\Delta P$ where 'Q' is the volumetric flow rate $\left(\frac{m^3}{s}\right)$, 'K' is paper permeability (m^2), 'A' is the cross sectional area of the paper normal to flow (m^2), 'µ' is the dynamic viscosity $\left(\frac{Ns}{m}\right)$, and 'ΔP' is the pressure drop $\left(\frac{N}{m^2}\right)$ occurring over a length 'L' (m) in the channel along the axis of flow. Darcy's Law assumes kinetic energy as negligible; the fiber cross section is circular, capillaries are straight and fluid properties remain constant. One dimensional fluid flow in porous networks during wetting can also be approximated (to the first order) by the Lucas Washburn equation assuming constant cross section/cylindrical pores, negligible gravitational effects, chemical homogeneity, and unlimited reservoir volume [79]:

$$x(t) = \sqrt{\frac{yrtcos\theta}{2\mu}} \qquad (1.1)$$

Where fluid with (liquid-vapor) surface tension 'y' $\left(\frac{\mathrm{N}}{\mathrm{m}}\right)$ and viscosity μ $\left(\frac{\mathrm{Ns}}{\mathrm{m}}\right)$, imbibes a distance 'x' in time 't', 'r' is capillary radius and 'θ' is the contact angle between the fluid and capillary wall. Fluid penetration distance increases with increasing effective capillary radius. Washburn's equation holds good for lateral flow as long as x<<z where 'z' is the height of fluid in a vertical column when the negative force of gravity is equal to the positive capillary force. The above equation is a first order approximation of fluid transport, and it tends to overestimate lateral wicking speed with fluid penetration distance. The variables which were not taken into account in above equation are the swelling that occurs in fibers during wetting, the increase in hydrodynamic resistance to flow during wetting, and that flow in paper networks is not straight (an assumption of the equation) but in actual it is not the case here. However these models were not specifically derived for fluid flow in paper, but they serve as a good approximation for describing simple systems, for example, single layer paper devices, simple geometries, horizontal orientation, and smaller gap heights.

As μPADs grow and becomes increasingly complex, these above described models become less applicable, especially for in-field testing where experimental conditions are more difficult to control or less than ideal (humidity, temperature etc.). This scenario was particularly highlighted for hollow channel or multilayered μPADs where a large proportion of fluid flow occurs between paper layers or layers of paper and other materials. Modeling the fluid dynamics for these hollow channel or multilayered μPAD systems is complicated by the multiple regions of flow, (i.e. in paper and gaps) as well as consideration of variables, such as gravity, which can normally be considered negligible in single layer μPAD designs, yet become critical when transporting larger volumes of fluids (hundreds of μL). Several studies have developed new models to address the limitations of above two equations toward complex μPAD designs. Martinez et al. derived a modified form of the Lucas Washburn equation to account for a 12 μm gap between two paper layers along with a consideration for humidity effects, which is given [17].

$$byl(t) = \sqrt{\frac{yr\varphi tcos\theta}{4q\mu}\left(1 - e^{-\frac{2qt}{\varphi t}}\right)} \qquad (1.2)$$

Where ‘t’ is the paper thickness, ‘q’ is the volumetric evaporation flux (the volume of evaporated liquid per unit area of wet channel and time), and ‘r’ is the area averaged effective pore size given by [17]:

$$r = \frac{2r't+2h^2}{2t+2h} \qquad (1.3)$$

where ‘2h’ is the gap height between the paper layers. Note, in the case of zero or negligible evaporation, q=0 and above equation simplifies to become Lucas Washburn equation. This equation works well for small gap heights (2h<=12), but provides a poor fit for gap heights greater than this. Toley et al. [20] employed the Richards equation [10] to model imbibition in µPADs. In that model Toley et al. [20] describes the paper as a series of partially saturated parallel capillaries. This model provides useful insights on flow in porous membranes, but requires multiple experiments and computational modeling in order to solve the equation for a new system, making it challenging to use. Berli et al. [23] have extended Lucas Washburn equation for devices of varying cross sectional areas, which are becoming more commonplace in complex µPAD designs. Kim et al. [75] have investigated the effect of hydrophobic boundaries such as wax on flow rates, providing a modified form of Lucas Washburn equation based on contact angles of the paper wax boundary. In the present study, we seek to provide a detail investigation toward establishing critical variables to the fast flow origins and model this behavior in multilayered µPADs with a universal equation that would be easy to use and extend the range of channel heights beyond those previously achieved.

Lucas Washburn equation and later its various modifications doesn’t explain the behavior of fluid flow through multilayered microPADs and it was explained in [73] that it is the sheer magnitude of Laplace pressure driving force in the gap between paper layers that is dragging the liquid in the paper layer and because of this Laplace pressure the flow in the region is dominated by the moving wall of the liquid at the gap boundary. Also this system behavior is not accurately predicted because of viscous dissipation effect within the paper layer that creates appreciable pressure lose. So the net pressure driving force in the Lucas Washburn equation [73] is:

$$\Delta P = P_c - P_v = \frac{y}{r}cos\theta - \frac{1}{Q}\int_v \mu\left(\frac{du_x}{dy}\right)^2 dV \qquad (1.4)$$

Where $= \frac{h}{cos\theta}$, 'Q' is the volumetric flow rate, 'u_x' is the liquid velocity component parallel to the channel boundaries in the paper layer, 'y' is the coordinate perpendicular to the boundaries, 'μ' is the liquid viscosity, and the integral is over the volume of liquid in the paper. Since 'u_x' is independent of 'x' at any time 't' and the slope of the velocity profile is constant in the paper, the integral can be directly evaluated to obtain [73]:

$$\Delta P = \frac{y}{r} cos\theta - t\mu \left(\frac{u}{t_h}\right)^2 \qquad (1.5)$$

Where '$u = \frac{dl}{dt}$' is the speed of the liquid front at any time 't' and 't_h' is the paper thickness.

Also there is always a room to do more research and brings fruitful results in every aspect of life so in our case one can work in many aspects like:-

- Theoretical modeling which accurately depicts behavior of fluid flow through multilayered (μPADs) considering all design parameters.
- To improve shelf life of reagents/enzymes stored on μPADs.
- To overcome Coffee Ring effect developed on paper material near hydrophobic boundary.
- Build a model on COMSOL Multiphysics to numerically analyze multilayered (μPADs).
- Perform multiple experiments using complex shaped Multilayered (μPADs) and observe behavior of all the design parameters involved in it.
- Manufacture paper having isotropic properties.

2 : LITERATURE REVIEW

Muller and Clegg (1949) patterned a filter paper with a paraffin barrier and observed that the confined channel sped up the sample diffusion process and reduced sample consumption. This research could be regarded as the basis of paper microfluidics [16]. Recent research in this area started in 2007 with the pioneering work of Martinez et al. (Andres W. Martinez S. T., 2007) on the development of µPADs. Martinez et al. [53], [82], [68], [31] have demonstrated that the processing of µPADs data can be done remotely because the colorimetric testing results could be scanned or photographed and transmitted electronically, which is particularly beneficial in environmental monitoring and analysis in remote areas by unskilled staff [4], [65], [8]. Evaluation of the analytical performance of µPADs [12] for the determination of reactive phosphate in soil solution showed that it was responsive over a wide concentration range, with excellent within and between device repeatability, and thus is suitable for the analysis of the range of soil and natural and marine waters. Previous studies have shown µPADs to be stable at room temperature for up to 24 h [12]. Whitesides and colleagues firstly used patterned paper to develop µPADs for bioanalytical applications [6], [7], [77], [91] with many advantages for satisfying the accessible and low cost requirements as follows: small volumes of reagents and samples, rapid analysis, portability, and easy to use and dispose of. In addition, the paper can be patterned into channels of hydrophilic surfaces separated by hydrophobic walls of photoresist [6], [7] polymer [19], wax [86], inks [44], and plasma treatment [84], etc. So it is clear that these µPADs are very attractive for point of care (POC) and on site diagnosis [21], [46], [81], [9]. Imbibition as type of capillary flow in porous media is a ubiquitous physical phenomenon, which has a wide range of applications from daily commodities, e.g., napkins and baby diapers, to advanced engineering applications, such as paper based chromatography [72], microfluidics for medical diagnosis [90], [74] energy harvesting devices [78], and oil recovery [64], [5]. The research on imbibition phenomena starts from the pioneer work by Lucas [47] and Washburn [79] who proposed an analytical model for capillary rise in tubes, known as Lucas Washburn equation. Motivated by limitations of the Lucas Washburn equation, a series of modification have been proposed, to consider the inertia [69], gravity [61], evaporation [61], and shape and tortuosity of the pore space (Jianchao Cai, 2014), [88]. These modified theoretical models

replenish the deviation between experimental results and predictions of the original Lucas Washburn equation, but the corresponding solutions are only available in one dimensional case. For higher dimensional cases, a few analytical solutions for homogeneous porous media of limited geometrical shapes are provided for radial penetration [58], [59] fan shape membrane [76], variable width paper strips [23], semi-infinite domain [39], and fractal porous media [87], [89]. Recently, the combined effects of geometry and evaporation and gravity are also investigated [60], [40]. Moreover, employing the nonlinear Richard's equation, [10] developed a two dimensional imbibition model that is suitable for arbitrary geometries of homogeneous porous media, i.e., effective properties are spatially independent. Imbibition in heterogeneous porous media is encountered commonly across different scales. For example, at the macro-scale, layered soils are typical heterogeneous porous media, which are composed of several layers of sediments characterized by grain and pore sizes [3], [45]. However, earlier work on overall flow properties of heterogeneous porous media [22], [67], [37] focuses on effective permeability instead of detailed imbibition processes, e.g., the evolution of liquid front, whilst recent work are mostly limited to layered configuration [41], [85], [1], [26], [70], [55], [51], [52]. Reyssat [51] conducted a research on the imbibition process of layered granular media experimentally and theoretically. Fernando [26] carried out a series of numerical simulations on a three layer porous media and adopted a hyperbolic tangent function to treat the interfaces approximately. In addition, at microscale, Michael [57] simulated the multicomponent flow in heterogeneous porous media through modified lattice Boltzmann method. Thus, it is necessary to extend the continuum numerical framework to more complex domains, in particular, solving problems with the presence of interfaces among distinct types of porous media. The capillary imbibition in heterogeneous porous media is much more complex than that in homogeneous ones. A generalized model is needed for quantitative prediction of these complex behaviors. The main challenge in the modeling process is to track the moving wetting front (i.e., the boundary between wetting and non-wetting fluids). In order to be applicable in complex-shaped domains, here we develop a model based on the fact that the liquid content, θ, around the wetting front shows a gradual change rather than a sharp transition, the value of θ is between zero and the porosity φ [32]. Thus, the degree of saturation, S, which varies from 0 to 1, is used to describe the partially occupied state of wetting phase in the pore space and taken as primary unknown.

Some researchers have demonstrated the physics of flow through porous media. They modeled the flow behavior by a linear relation of pressure gradient versus flow velocity (Darcy regime) in cases where the flow is dominated by viscous effects. When the flow velocity becomes adequately large, they used a nonlinear relation to include the inertial effects. Some researchers attempt to use theoretical methods to correlate with experimental data. The two best known theoretical relations are the Forchheimer equation and Ergun or Ergun-type equations. Both are widely used as there is no specific reason for choosing one rather than the other. Early works by [28], [29] reported that the flow pressure characteristics of porous media can be represented by a dimensionless expression related to the square root of the permeability. Montellit [2] extended the applicability of an existing correlating equation to predict the pressure drop through packed beds of spheres. Antohe [15] proposed a more precise method based on curve fitting to calculate the permeability and inertia coefficients of porous matrices in terms of a Forchheimer flow model. Dukhan and Minjeur [33] found that the permeability for the Darcy regime differs from that for the Forchheimer regime. Liu [34] developed an Ergun-type empirical equation to correlate the dimensionless pressure drop with flow velocity for several types of foam matrix porous media. Dukhan and Patel [63] correlated the permeability and the form drag coefficient using an Ergun model with the reciprocal of the surface area density, which has a unit of $\frac{m^3}{m^2}$, indicating that it is used as an equivalent length scale. Dietrich et al. [13] presented experimental data of pressure drop measurements of different ceramic sponges and determined the two constants of the Ergun equation, which are verified to be independent of the material and porosity. The Forchheimer and Ergun equations look very similar in that they both have a viscous term and an inertia term. The difference is that the Forchheimer equation uses an analogy with pipe flow while the Ergun equation models the space between packed beds of spheres as parallel capillaries. Existing studies proved that the Darcy-Forchheimer-based theory can be applied to both compressible and incompressible fluids.

Moving mesh simulations were carried out to study the absorption of the fluid in the cellulosic fiber networks of paper substrate [76]. Studies were also performed to find out the permeability of air in cellulosic fibers and derived different empirical relations to find out the relative permeability [71]. From the experimental studies carried out by Chiou and Smith, it was found that the adsorption constant of material is different for different solutes and also it varies with the

grade of paper used for making the device [83]. A major problem faced in µPADs for sensing application is the distribution of reagent after the sampling [82]. It was observed that the immobilized reagents swept away by the sample solution and which leads to non-uniformity or reagent over the substrate. Hence it is difficult to locate the exact position of the substrate where the maximum concentration of reagent occurs.

From portable sensor requirements perspectives, microfluidic devices are significantly appealing technologies to achieve the Lab-on-a-chip (LoC) based point of care applications [66], [42]. It is possible to perform multiple analyses on the microfluidic platform by just modifying its microchannel patterns. Micromixers have a pivotal point in enhancing the sensitivity of the microfluidic based sensors [35], [24], [62]. By stacking layers of patterned paper it is possible to create three dimensional (3D) vertical and lateral microfluidic systems thus significantly expanding the capabilities of µPADs. Different techniques can be used to assemble the 3D µPADs, which consist of either sticking individual layers of patterned paper together using adhesive tape or spray, or simply folding a single layer of patterned paper. The latter is known as origami method and has the advantage of eliminating possible contamination issues originated from the use of adhesives [24]. There are different types of paper employed in paper based sensors depending on the fabrication method and the application of the sensor. The most extensively used material is Whatman brand chromatography paper due to its superior wicking ability [9], [11], [14], [54]. This particular type of paper has medium retention rate and flow rate owing to its thickness (180 µm) and pore size (11 µm). Other types of paper such as the Whatman filter paper No. 4, was used due to its larger pore size of 20-25 µm and higher retention rate [50]. The use of origami (folding of paper) [49] and kirigami (cutting of paper) [14] techniques during the fabrication of microfluidic devices has given researchers new opportunities for fabricating their devices. The principles of origami were used to create a unique device in which two zones are separated by a crease [49]. One zone is the detection zone and the other is the enzyme immobilization zone. In this work, the researchers designed a paper based analytical device to electrochemically detect glucose using an origami-inspired device [80].

3 : METHODOLOGY

In our methodology COMSOL Multiphysics Software has been adopted in order to perform numerical analysis of impact of various design parameters on single layered and multilayered microfluidic paper based analytical device (μPADs), and also for the third portion, MATLAB Software has been used to simulate ODEs with boundary and initial conditions obtained from Experimental work of Robert B. Channon research paper [73]. COMSOL Multiphysics Software is general purpose simulation software based on advanced numerical methods. It has fully coupled multiphysics and single physics modeling capabilities. It has complete modeling workflow, from geometry to post-processing. It has user-friendly tools for building and deploying simulation apps.

The need for advanced porous media modeling spans many industries. The Porous Media Flow Module, was made for this: it lets you quantitatively investigate mass, momentum, and energy transport in porous media. Interest areas for this product include fuel cell processes, pulp and paper drying, the production of food, filtration, and many more.

Simulating mass, momentum, and energy flow in porous media is common in a number of engineering fields, such as chemical, civil, and nuclear engineering. The Porous Media Flow Module provides a comprehensive set of physics interfaces to help engineers and scientists simulate different types of physical processes in porous media.

MATLAB is a programming and numeric computing platform used by engineers and scientists to analyze data, develop algorithms, and create models.

3.1 Multiphase Transport in Porous Media:

The Porous Media Flow Module includes tools that can be used to simulate multiphase flow in porous media with two or any number of moving phases. We can specify porous media properties such as relative permeability's and capillary pressures between phases to model wicking, moisture transport, or other transport phenomena in porous media.

3.1.1 Darcy's Law interface:

The Darcy's Law interface, found under the Porous Media and Subsurface Flow branch when adding a physics interface, is used to simulate fluid flow through interstices in a porous medium. It can be used to model low-velocity flows or media where the permeability and porosity are very small, and for which the pressure gradient is the major driving force and the flow is mostly influenced by the frictional resistance within the pores [43].

$$u_i = -\frac{K_{ri}}{\mu_i} K(\nabla p_i - \rho_i g) \qquad (3.1)$$

3.1.2 Governing Equations of Phase Transport in Porous Media:

The Phase Transport and Phase Transport in Porous Media interfaces are intended for studying the transport of multiple immiscible fluid, gas or (dispersed) solid phases either in free flow or flow through a porous medium. The interfaces solve for the averaged volume fractions (also called saturations in a porous medium) of the phases, and does not track the interfaces between the different phases. Both interfaces are based on the macroscopic mass conservation equations of each phase. In a porous medium the effects of the microscopic (or pore scale) interfaces between the phases can be taken into account via the capillary pressure functions.

In the porous domain, the mass conservation equation for each phase is given by [36]:

$$\frac{\partial}{\partial t} E_p \rho_i s_i + \nabla . (\rho_i u_i) = Q_i \qquad (3.2)$$

Here 'E_p'(dimensionless) is the porosity, and the vector u_i should now be interpreted as the volumetric flux of phase i (SI unit $m^3/(m^2.s)$ or m/s). The volumetric fluxes are determined using the extended Darcy's Law [84].

$$u_i = -\frac{K_{ri}}{\mu_i} K(\nabla p_i - \rho_i g) \qquad (3.3)$$

Where 'K' denotes the permeability (SI unit: m^2) of the porous medium, 'g' is the gravitational acceleration vector (SI unit: m/s^2), 'μ_i' the dynamic viscosity (SI unit: kg/(m.s)), p_i the pressure field (SI Unit: Pa), and 'K_{ri}' the relative permeability (dimensionless) of phase i, respectively.

One phase pressure can be chosen independently, which in the Phase transport in porous media interface is chosen to be the phase pressure, 'p_{i_c}', of the phase computed from the volume constraint, and the other phase pressures are defined by the following 'N-1' capillary pressure relations [30]:

$$p_i = p_{i_c} + p_{c_i}(s_1, \dots \dots s_N) \qquad for\ i \neq i_c \qquad (3.4)$$

Substituting (3.2) into (3.1) and using the volume constraint $\sum_{i=1}^{N} s_i = 1$ we arrive at the following N-1 equations for the phase volume fractions s_i, ($i \neq i_c$) that are solved in the Phase transport in porous media interface:

$$\frac{\partial}{\partial t} E_p \rho_i s_i - \nabla . \left(\rho_i K_{ri} \left(\nabla \left(p_{i_c} + p_{c_i} \right) - \rho_i g \right) \right) = Q_i \qquad (3.5)$$

The remaining volume fraction is computed from [30]:

$$s_{i_c} = 1 - \left(\sum_{i=1, i \neq i_c}^{N} s_i \right) \qquad (3.6)$$

3.2 Governing Equations of Free and Porous Media Flow Interface:

The Free and porous media flow interface uses the Navier–Stokes equations to describe the flow in open regions, and the Brinkman equations to describe the flow in porous regions.

Flow in the free channel is described by the time dependent, incompressible Navier-Stokes equations [48]:

$$\rho \frac{\partial u}{\partial t} + \rho (u . \nabla) u = \nabla . [-pI + K] + F \qquad (3.7)$$

$$\rho \nabla . (u) = 0 \qquad (3.8)$$

$$K = \mu (\nabla u + (\nabla u)^T) \qquad (3.9)$$

$$\rho \frac{\partial u}{\partial t} + \rho (u . \nabla) u = \nabla . [-pI + \mu (\nabla u + (\nabla u)^T)] + F \qquad (3.10)$$

Where 'μ' denotes the dynamic viscosity (Pa.s), 'u' refers to the velocity in the open channel (m/s), 'ρ' is the fluid's density (kg/m^3), and 'p' is the pressure (Pa). In the porous domain, the Brinkman equations describe the flow:

The dependent variables in the Brinkman equations are the Darcy velocity and the pressure. The flow in porous media is governed by a combination of the continuity equation and the momentum equation, which together form the Brinkman equations [36]:

$$\frac{\partial}{\partial t}(E_p \rho) + \nabla.(\rho u) = Q_m \qquad (3.11)$$

$$\frac{\rho}{E_p}\left(\frac{\partial u}{\partial t} + \frac{(u.\nabla)u}{E_p}\right) = -\nabla p + \nabla.\left[\frac{1}{E_p}\left\{\mu(\nabla u + (\nabla u)^T) - \frac{2}{3}\mu(\nabla.u)I\right\}\right] - \left(K^{-1}\mu + \frac{Q_m}{E_p^2}\right)u + F \qquad (3.12)$$

It is the sheer magnitude of the Laplace pressure driving force in the gap between the paper layers that the flow in the gap is dragging the liquid in the paper layer and the flow in that region is dominated by the "moving wall" of the liquid at the gap boundary. If the capillary pressure driving force in the gap is denoted as 'P_c' and the pressure loss due to viscous dissipation is 'P_v', then the net pressure driving force in the Lucas-Washburn formulation [73] is:

$$\Delta P = P_c - P_v = \frac{y}{r}cos\theta - \frac{1}{Q}\int_v \mu\left(\frac{du_x}{dy}\right)^2 dV \qquad (3.13)$$

Where '$r = \frac{h}{cos\theta}$', 'Q' is the volumetric flow rate, 'u' is the liquid velocity component parallel to the channel boundaries in the paper layer, 'y' is the coordinate perpendicular to the boundaries, 'μ' is the liquid viscosity, and the integral is over the volume of liquid in the paper. Since 'u_x' is independent of 'x' at any time and the slope of the velocity profile is constant in the paper, the integral can be directly evaluated to obtain [73]:

$$\Delta P = \frac{y}{r}cos\theta - t\mu\left(\frac{u}{t_h}\right)^2 \qquad (3.14)$$

Free and Porous Media interface has been used for numerical analysis of multilayered microfluidic paper based analytical device.

Parameters involved in both single and multilayered μPADs are listed below but with every different Whatman filter paper porosity, permeability and pore radius value changes:

Parameters

Name	Expression	Value	Description
L0	0.12[m]	0.12 m	Paper strip height
W0	0.02[m]	0.02 m	Paper strip width
th	2e-4[m]	2E-4 m	Paper strip thickness
gamma	0.0723[N/m]	0.0723 N/m	Surface tension
theta	141[degree]	2.4609 rad	Contact angle
Rc	1.1e-6[m]	1.1E-6 m	Pore radius
pec	-2*gamma*cos(theta)...	1.0216E5 N/m^2	Entry capillary pressure
lp	2	2	Pore size distribution index
por	0.54	0.54	Porosity
K	1.5e-14 [m^2]	1.5E-14 m^2	Permeability
rho_air	1[kg/m^3]	1 kg/m^3	Air density
rho_water	1e3[kg/m^3]	1000 kg/m^3	Water density
mu_air	1.76e-5[Pa*s]	1.76E-5 Pa·s	Air viscosity
mu_water	8.9e-4[Pa*s]	8.9E-4 Pa·s	Water viscosity

Figure 3.1: Parameters used for single and multilayered µPADs numerical analysis

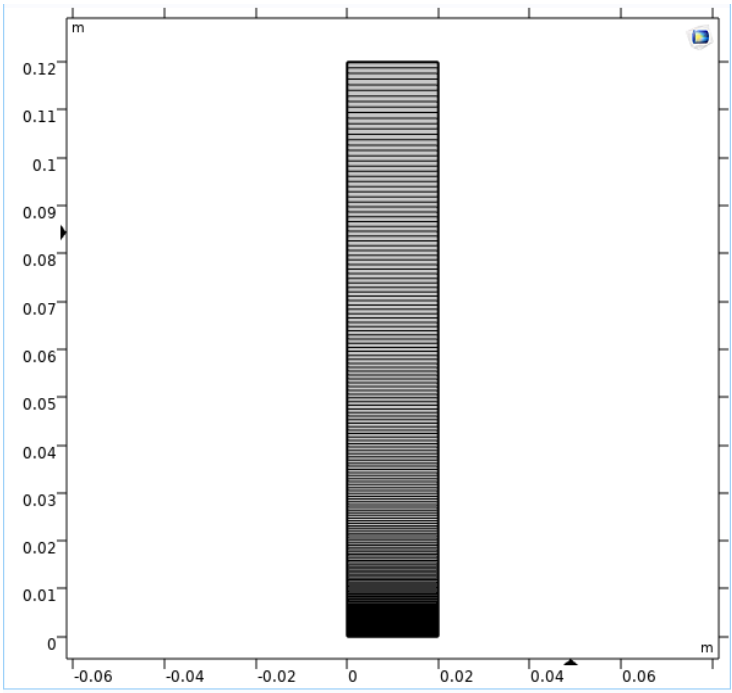

Figure 0.1: Mesh of single layered µPADs

4 : RESULTS AND DISCUSSION

While using "Multiphase Flow in Porous Media" interface for single layer µPADs using COMSOL Multiphysics software, below are the results:

Parameters which have been selected for Whatman filter paper grade 1 are mentioned below:

4.1 Whatman filter paper grade 1:

.

Parameters

Name	Expression	Value	Description
L0	0.12[m]	0.12 m	Paper strip height
W0	0.02[m]	0.02 m	Paper strip width
th	1.8e-4[m]	1.8E-4 m	Paper strip thickness
gamma	0.0723[N/m]	0.0723 N/m	Surface tension
theta	0	0	Contact angle
Rc	5.5e-6 [m]	5.5E-6 m	Pore radius
pec	2*gamma*cos(theta)/Rc	26291 N/m^2	Entry capillary pressure
lp	2	2	Pore size distribution index
por	0.48	0.48	Porosity
K	9.81e-14[m^2]	9.81E-14 m^2	Permeability
rho_air	1[kg/m^3]	1 kg/m^3	Air density
rho_water	1e3[kg/m^3]	1000 kg/m^3	Water density
mu_air	1.76e-5[Pa*s]	1.76E-5 Pa·s	Air viscosity
mu_water	8.9e-4[Pa*s]	8.9E-4 Pa·s	Water viscosity

Figure 4.1: Parameters used for numerical analysis of single layered Whatman filter paper

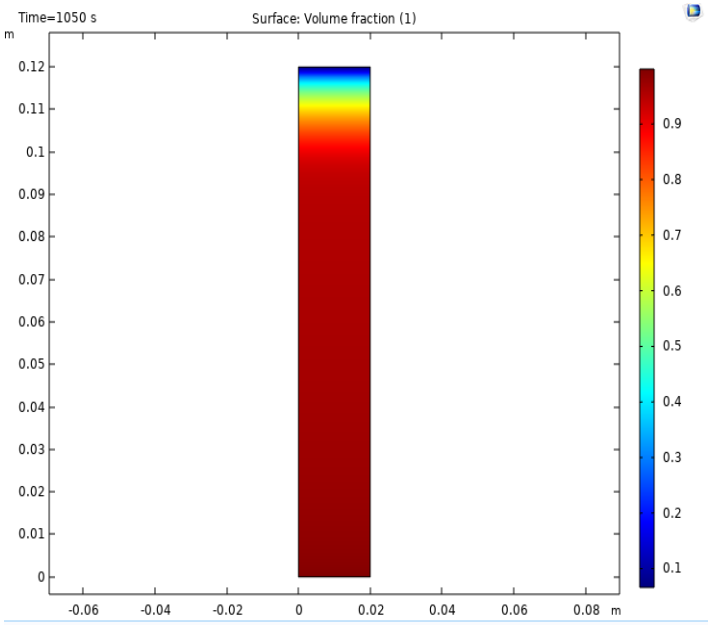

Figure 4.2:Volume fraction plot of Whatman filter paper grade 1

Volume fraction plot depicts volume of fluid taken by paper during wicking with respect to time. Interface develops between both phases (air and water) and its value is 1 for one phase and 0 for other phase and in between value is used where interference of both phases occurred.

Surface pressure plot gives us how capillary pressure value at different points causes the fluid to lift upward against gravity.

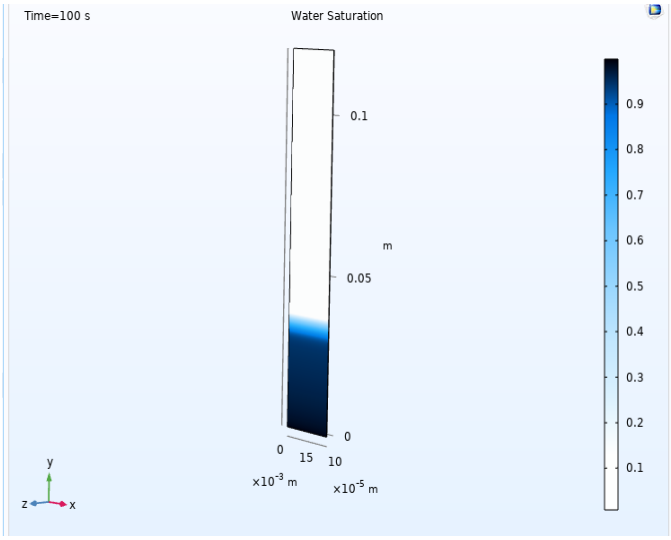

Figure 4.4: Water saturation in 3D

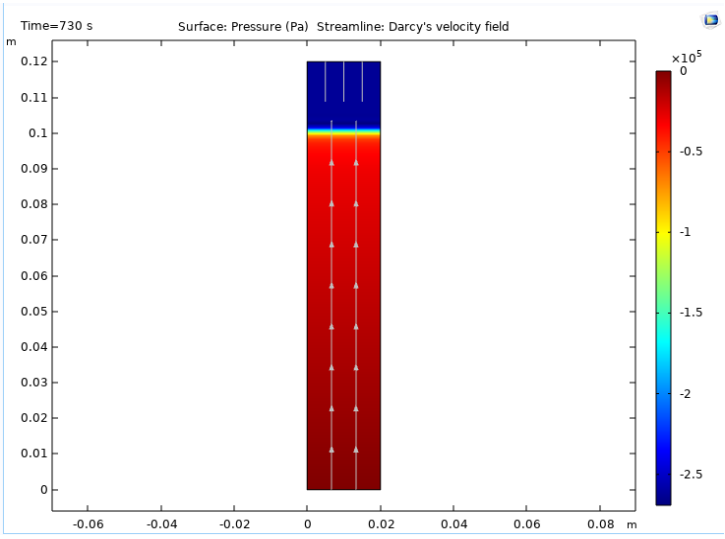

Figure 4.3: Surface pressure, streamline Darcy's velocity field

It takes 1050s for the fluid to reach at maximum height of 0.12 m.

4.2 Whatman filter paper grade 3:

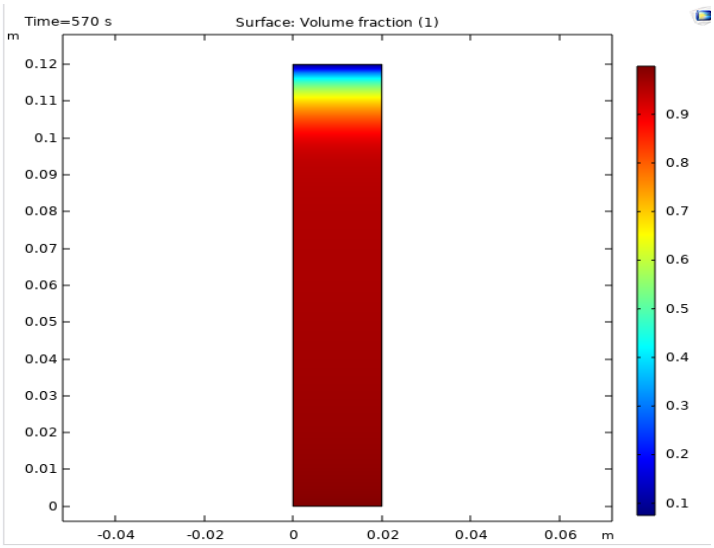

Figure 4.5: Volume fraction plot of Whatman filter paper grade 3

Parameters

Name	Expression	Value	Description
L0	0.12[m]	0.12 m	Paper strip height
W0	0.02[m]	0.02 m	Paper strip width
th	390e-6[m]	3.9E-4 m	Paper strip thickness
gamma	0.0723[N/m]	0.0723 N/m	Surface tension
theta	0	0	Contact angle
Rc	3e-6 [m]	3E-6 m	Pore radius
pec	2*gamma*cos(theta)/Rc	48200 N/m^2	Entry capillary pressure
lp	2	2	Pore size distribution index
por	0.77	0.77	Porosity
K	1.57e-13	1.57E-13	Permeability
rho_air	1[kg/m^3]	1 kg/m^3	Air density
rho_water	1e3[kg/m^3]	1000 kg/m^3	Water density
mu_air	1.76e-5[Pa*s]	1.76E-5 Pa·s	Air viscosity
mu_water	8.9e-4[Pa*s]	8.9E-4 Pa·s	Water viscosity

Figure 4.6: Parameters used for numerical analysis of single layered Whatman filter paper

It takes 570s for the fluid to reach at maximum height of 0.12 m

4.3 Whatman Filter Paper Grade 4:

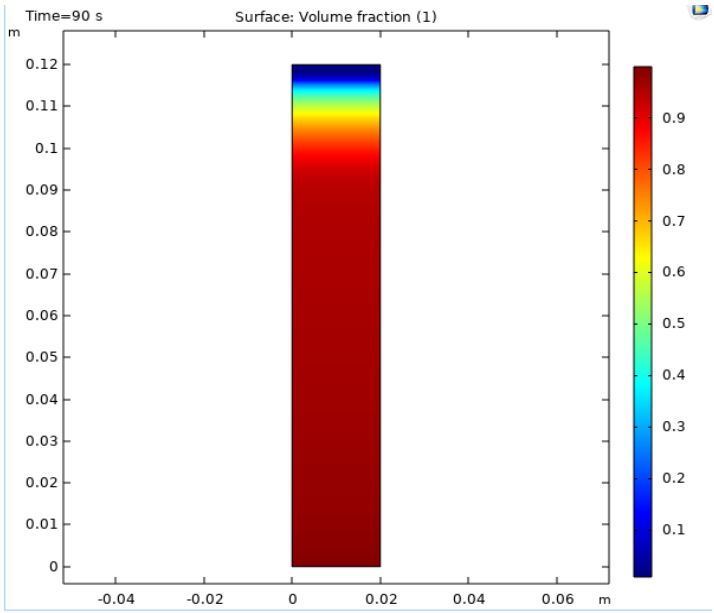

Figure 4.7: Volume fraction plot of whatman filter paper grade 4

Parameters

Name	Expression	Value	Description
L0	0.12[m]	0.12 m	Paper strip height
W0	0.02[m]	0.02 m	Paper strip width
th	205e-6[m]	2.05E-4 m	Paper strip thickness
gamma	0.0723[N/m]	0.0723 N/m	Surface tension
theta	0	0	Contact angle
Rc	25e-6[m]	2.5E-5 m	Pore radius
pec	2*gamma*cos(theta)/Rc	5784 N/m^2	Entry capillary pressure
lp	2	2	Pore size distribution index
por	0.776	0.776	Porosity
K	8.67e-12	8.67E-12	Permeability
rho_air	1[kg/m^3]	1 kg/m^3	Air density
rho_water	1e3[kg/m^3]	1000 kg/m^3	Water density
mu_air	1.76e-5[Pa*s]	1.76E-5 Pa·s	Air viscosity
mu_water	8.9e-4[Pa*s]	8.9E-4 Pa·s	Water viscosity

Figure 4.8: Parameters used for numerical analysis of single layered Whatman filter paper

It takes 90s for the fluid to reach at maximum height of 0.12 m.

4.4 Whatman filter paper grade 5:

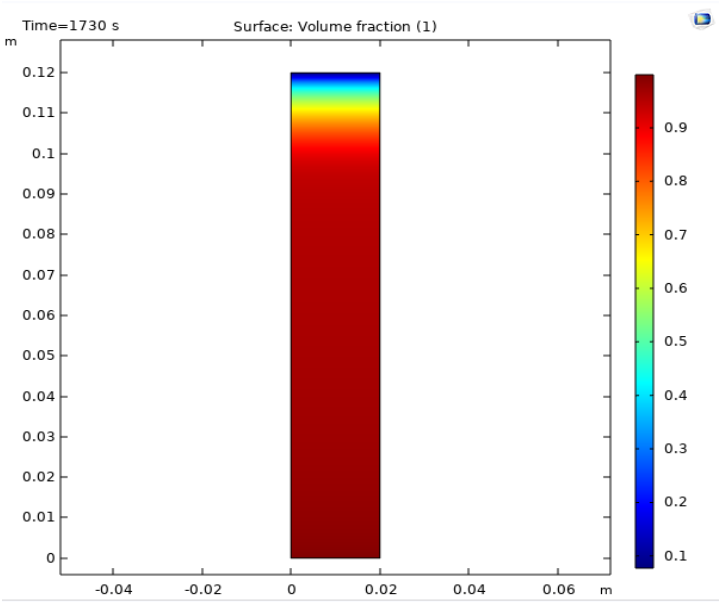

Figure 4.9: Volume fraction plot of Whatman filter paper grade 5

Parameters

Name	Expression	Value	Description
L0	0.12[m]	0.12 m	Paper strip height
W0	0.02[m]	0.02 m	Paper strip width
th	2e-4[m]	2E-4 m	Paper strip thickness
gamma	0.0723[N/m]	0.0723 N/m	Surface tension
theta	0	0	Contact angle
Rc	1.25e-6[m]	1.25E-6 m	Pore radius
pec	2*gamma*cos(theta)/Rc	1.1568E5 N/m^2	Entry capillary pressure
lp	2	2	Pore size distribution index
por	0.54	0.54	Porosity
K	1.5e-14[m^2]	1.5E-14 m^2	Permeability
rho_air	1[kg/m^3]	1 kg/m^3	Air density
rho_water	1e3[kg/m^3]	1000 kg/m^3	Water density
mu_air	1.76e-5[Pa*s]	1.76E-5 Pa·s	Air viscosity
mu_water	8.9e-4[Pa*s]	8.9E-4 Pa·s	Water viscosity

Figure 4.10: Parameters used for numerical analysis of single layered Whatman filter paper grade 5

It takes 1730s for the fluid to reach at maximum height of 0.12 m. Whatman filter paper grade 4 allows fluid to takes less time to reach certain height because of its high permeability value.

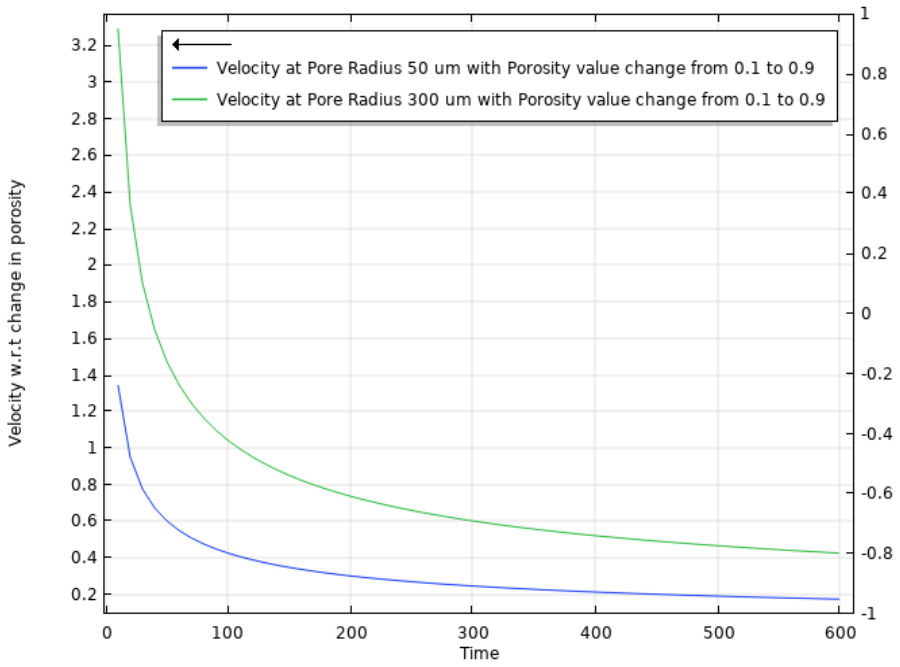

Figure 4.11: Velocity VS Time graph for two different pore radius and at different porosity value from 0 to 0.9

Above graph shows that velocity of fluid through porous media has no effect due to change in porosity value or we can say that it doesn't depend on it, however it does depends on pore radius and it has direct relation with it means by increasing pore radius velocity magnitude becomes enhanced in start and remain heighten throughout its penetration in paper layer as compared to paper layer with small pore radius.

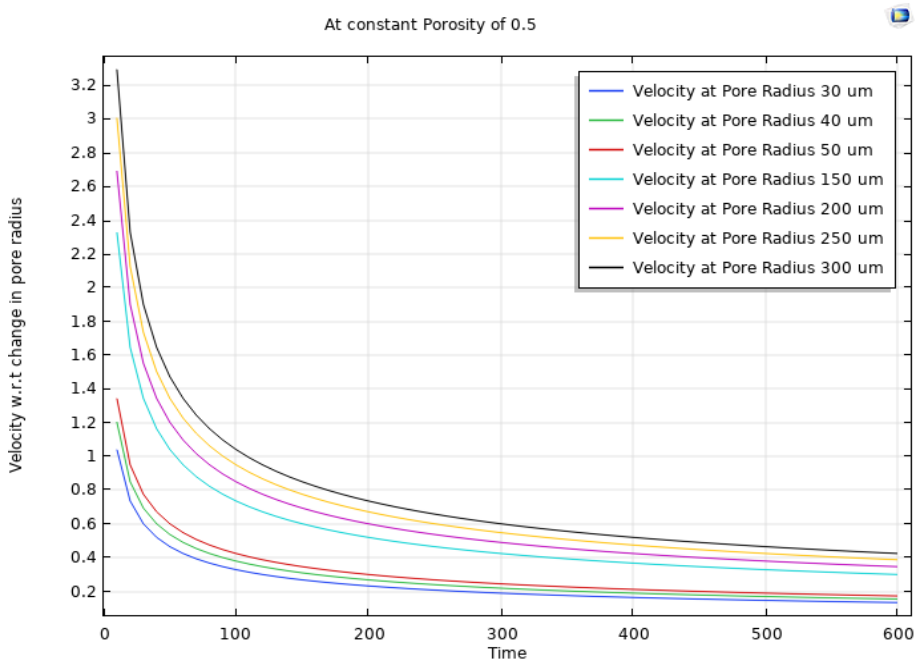

Figure 4.12: Velocity VS Time graph for seven different pore radius and at constant porosity value of 0.5

Above graph shows that velocity of fluid through porous medium has direct relation with Pore radius as we can see that with increase in pore radius, velocity enhancement has been seen in its journey.

Now using “Free and Porous Media Domain” model for multilayered microPADs.

Whatman filter paper grade 4 properties has been used with initial and boundary conditions as mentioned below:

- Inlet velocity of fluid = 0.01 m/s
- Outlet pressure = 101325 Pa or 0 Pa
- Initial value in fluid domain = 101325 Pa or 0 Pa
- Initial value in porous domain = Capillary pressure
- Paper strip thickness = 210 um
- Fluid passage height = 312 um

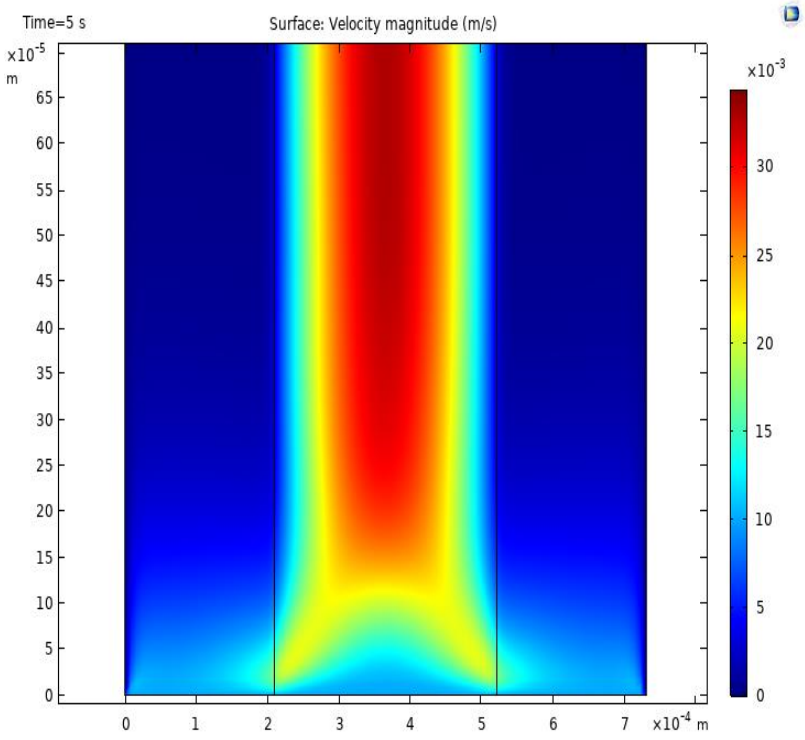

Figure 4.13: Surface plot of Velocity magnitude

Name	Expression	Value	Description
L0	10[cm]	0.1 m	Paper Strip Height
gamma	0.0728[N/m]	0.0728 N/m	Surface Tension
theta	34[degree]	0.59341 rad	Contact Angle
Rc	25e-6[m]	2.5E-5 m	Pore Radius
pec	(2*gamma*cos(t...	4828.3 N/m^2	Entry Capillary Pressure
por	0.9	0.9	Porosity
K	por/8*Rc^2	7.0313E-11 m^2	Permeability
rho_air	1[kg/m^3]	1 kg/m^3	Air density
rho_water	1e3[kg/m^3]	1000 kg/m^3	Water density
mu_air	1.76e-5[Pa*s]	1.76E-5 Pa·s	Air viscosity
mu_water	0.001[Pa*s]	0.001 Pa·s	Water viscosity

Figure 4.14: Whatman filter paper grade 4 properties used for numerical analysis of multilayered µPADs

4.5 Solving ODEs obtained from Experiments performed on Multilayered µPADs using MATLAB Software:

In addition to analyzing the effect of four different parameters on the velocity profile e.g. capillary angle, dynamic viscosity, surface tension, paper thickness etc. the impact of gap heights was also examined. In addition, the validation results are also presented.

The results are as follows:

4.5.1 Validation results:

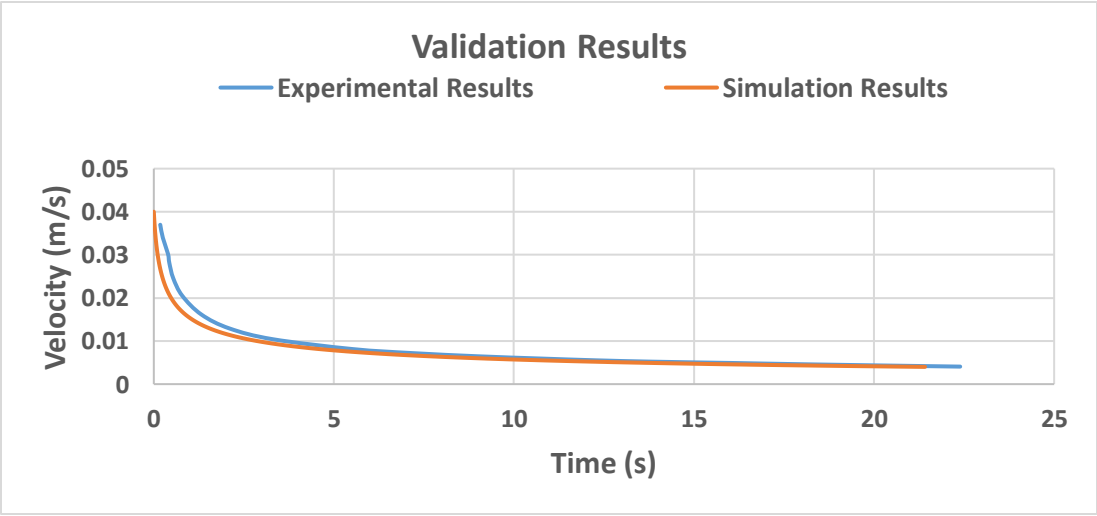

Figure 4.15: Comparison of Experimental and Simulation results for gap height of 234 µm

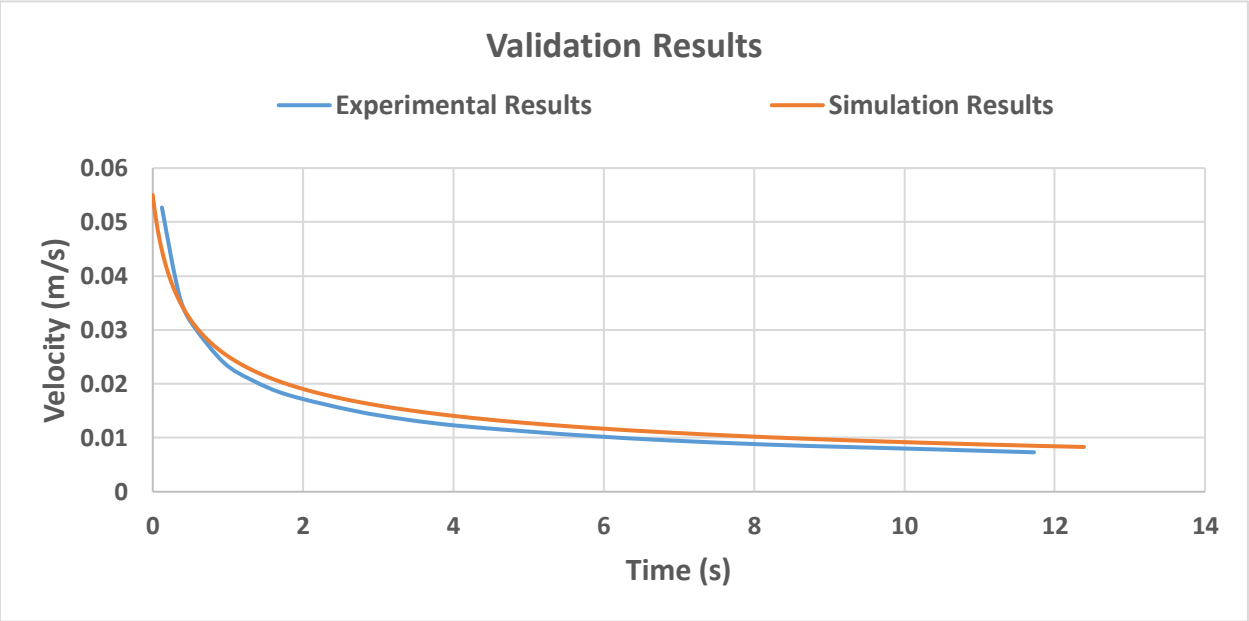

Figure 4.16: Comparison of Experimental and Simulation results for gap height of 312 µm

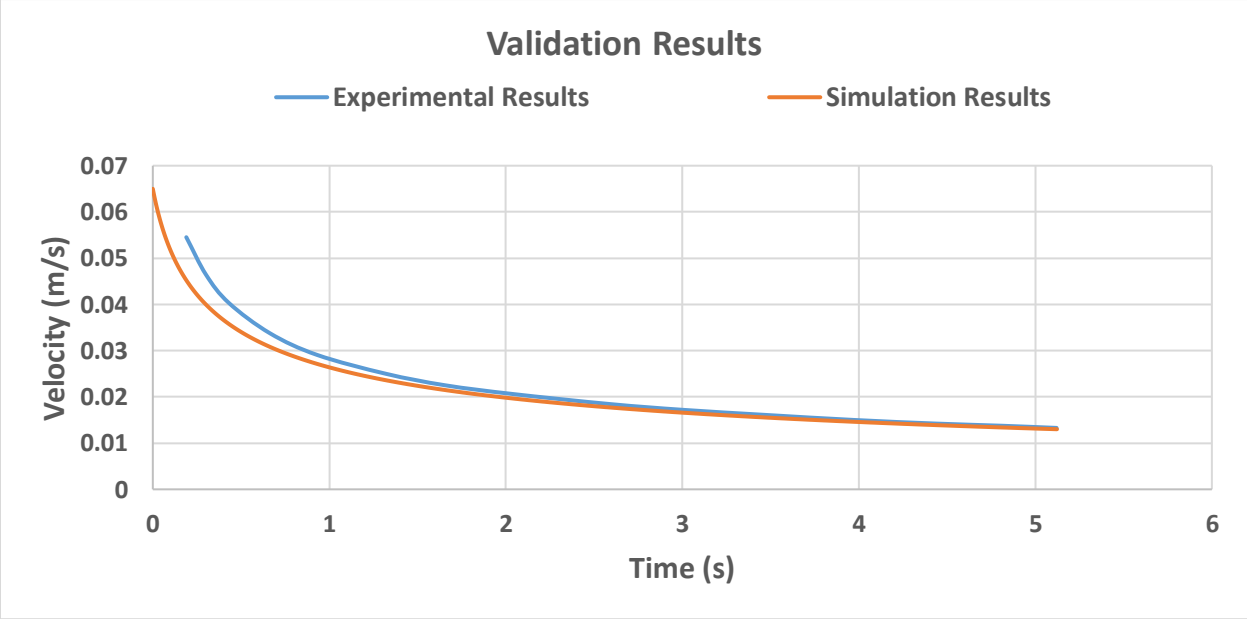

Figure 4.18: Comparison of Experimental and Simulation results for gap height of 390 µm

As can be seen from above figures, the simulation results/ODEs are in good agreement with the experimental data which is taken from Robert B. Channon et al. [73].

4.5.2 Effect of interfacial tension:

Below graphs illustrates how interfacial tension affects velocity profiles at three different gap heights.

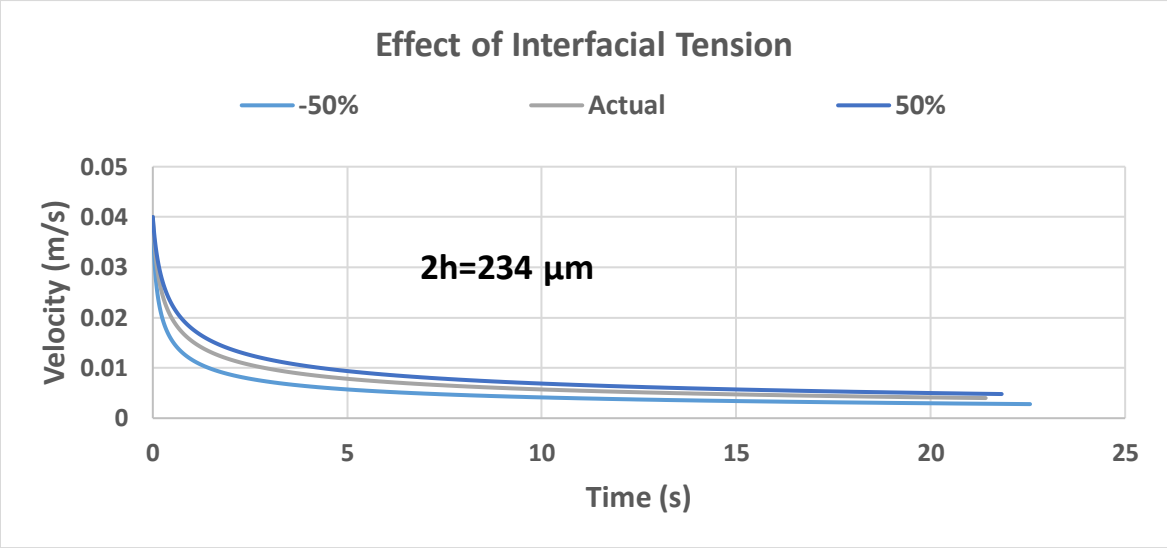

Figure 4.20: Velocity VS Time for 234 µm gap height with 03 different interfacial tension values

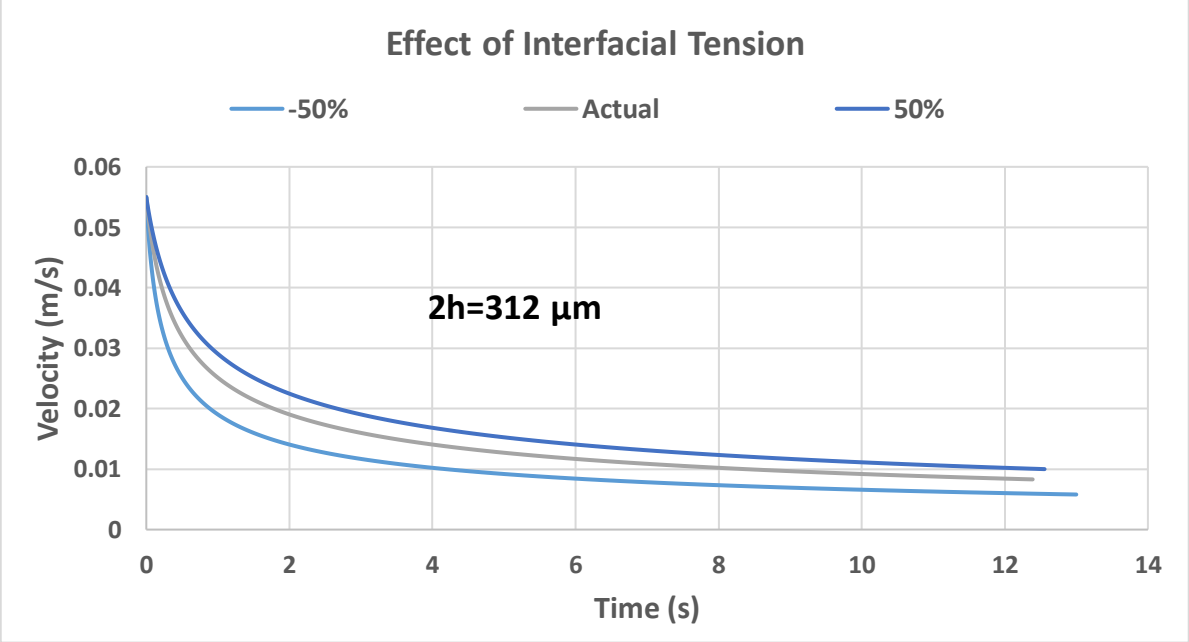

Figure 4.19: Velocity VS Time for 312 µm gap height with 03 different interfacial tension values

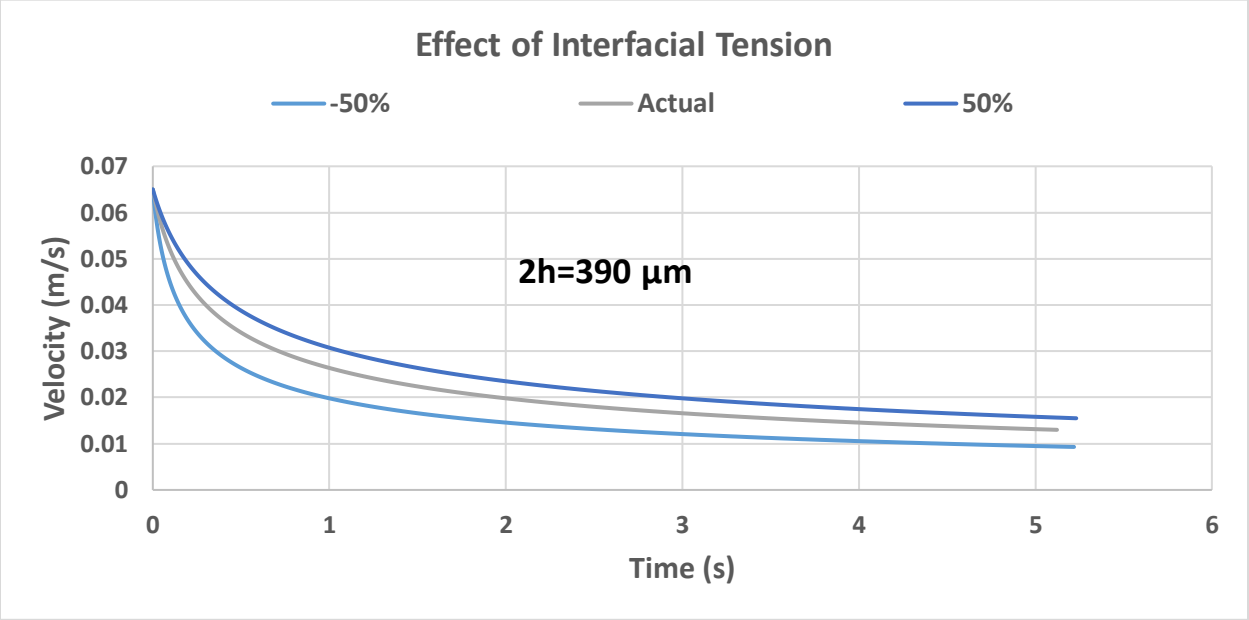

Figure 4.21: Velocity VS Time for 390 µm gap height with 03 different interfacial tension values

Velocity of fluid is found to be directly proportional to interfacial tension because it helps fluid to hold the surface intact. Hence increase in surface tension causes increase in velocity of fluid.

4.5.3 Effect of fluid dynamic viscosity:

The effect of fluid dynamic viscosity on velocity profile is presented in below figures.

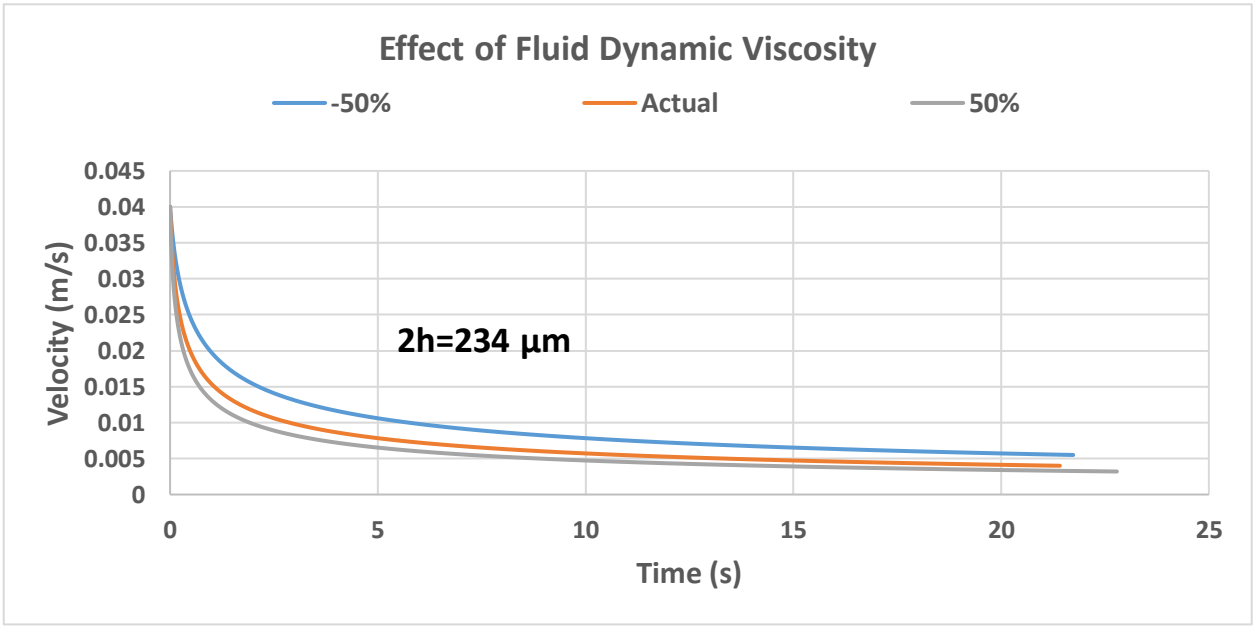

Figure 4.22: Velocity VS Time for 234 µm gap height with 03 different dynamic viscosity values

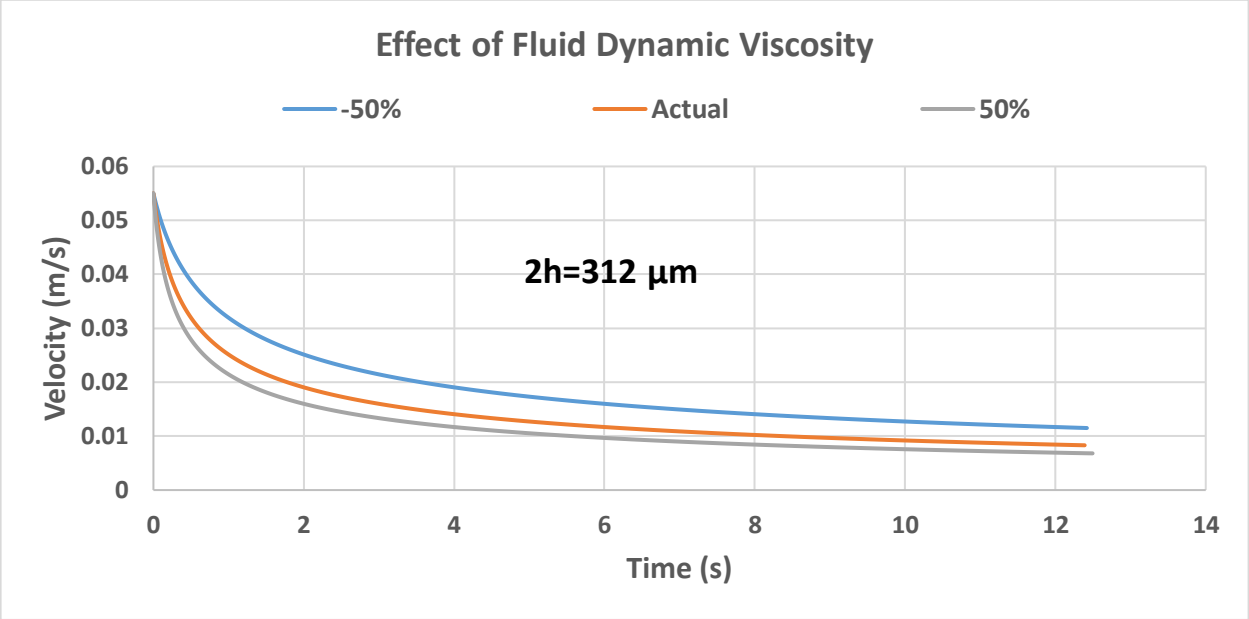

Figure 4.23: Velocity VS Time for 312 µm gap height with 03 different dynamic viscosity values

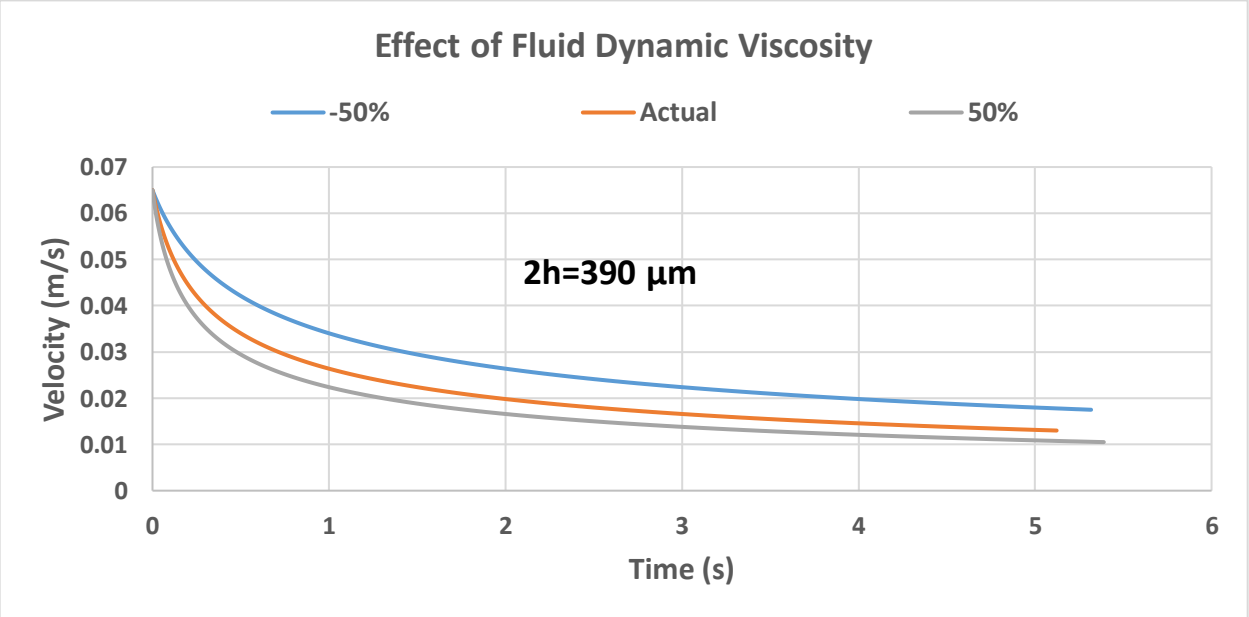

Figure 4.24: Velocity VS Time for 390 µm gap height with 03 different dynamic viscosity values

Dynamic viscosity plays a negative role in terms of change in velocity because it creates hindrance to fluid flow so increase in viscosity causes decrease in velocity.

4.5.4 Effect of paper thickness:

As shown in below figures, changes in paper thickness affected the velocity profile.

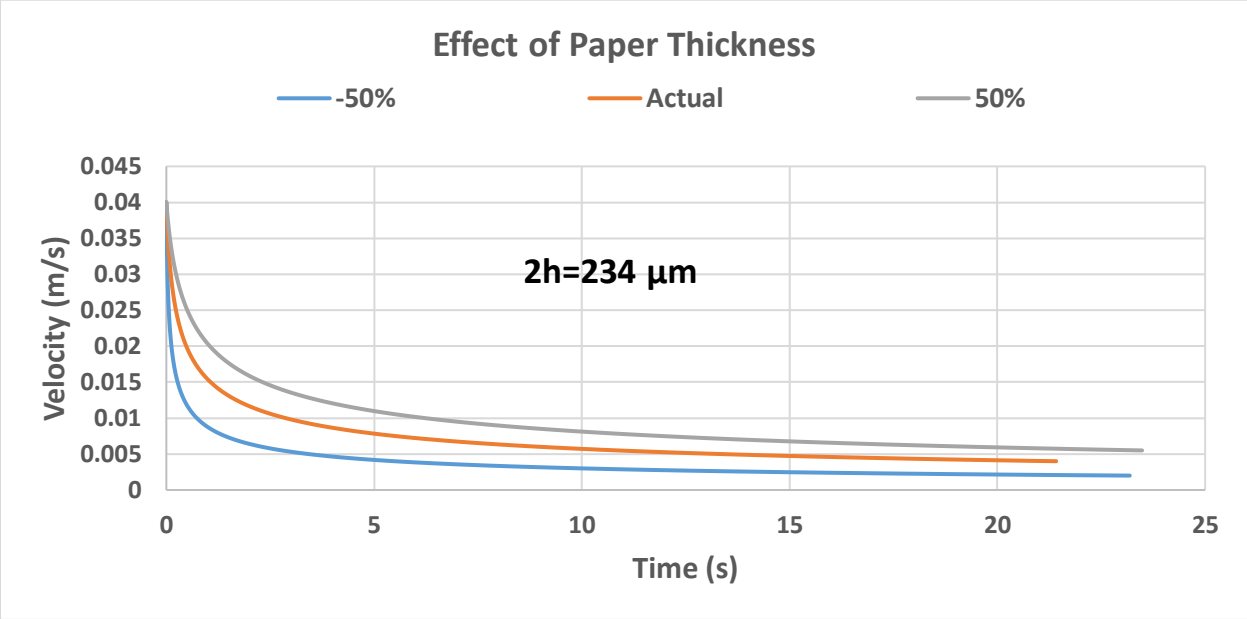

Figure 4.25: Velocity VS Time for 234 µm gap height with 03 different paper thickness

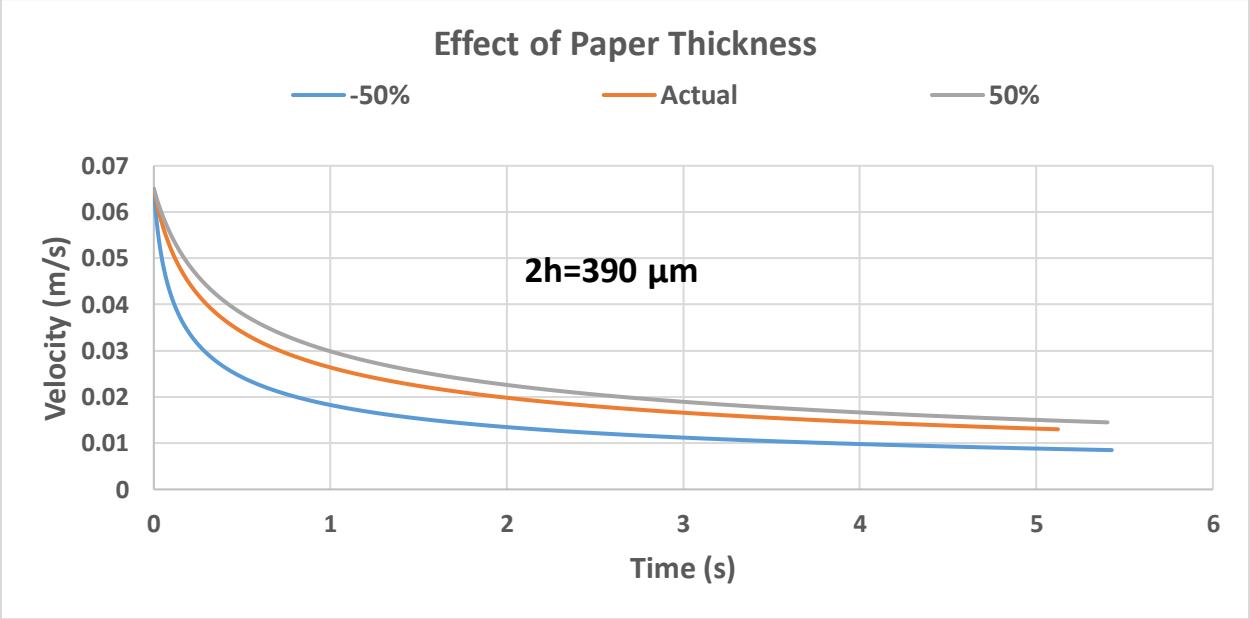

Figure 4.26: Velocity VS Time for 390 µm gap height with 03 different paper thickness

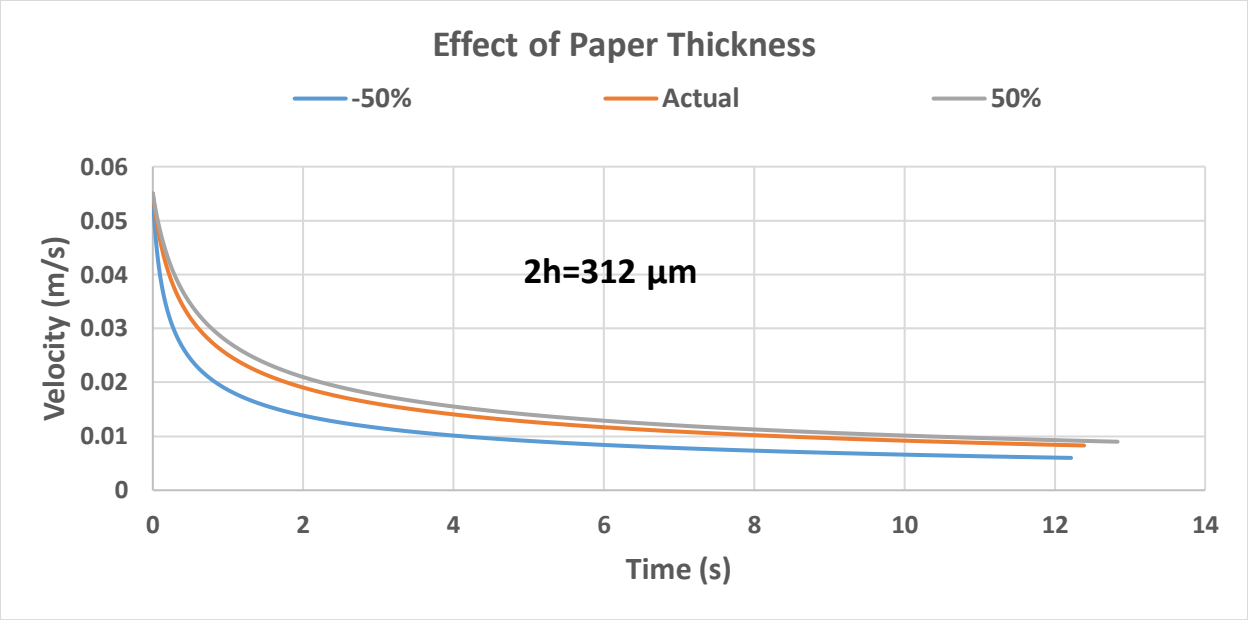

Figure 4.27: Velocity VS Time for 312 µm gap height with 03 different paper thickness

Paper thickness plays a positive role in terms of increase in velocity because paper thickness effects pore radius and permeability value which we have found in case of single layer µPADs, that they are directly proportional to increase in velocity.

4.5.5 Effect of fluid contact angle on paper:

Below figures shows the effect of the fluid contact angle on the velocity profile.

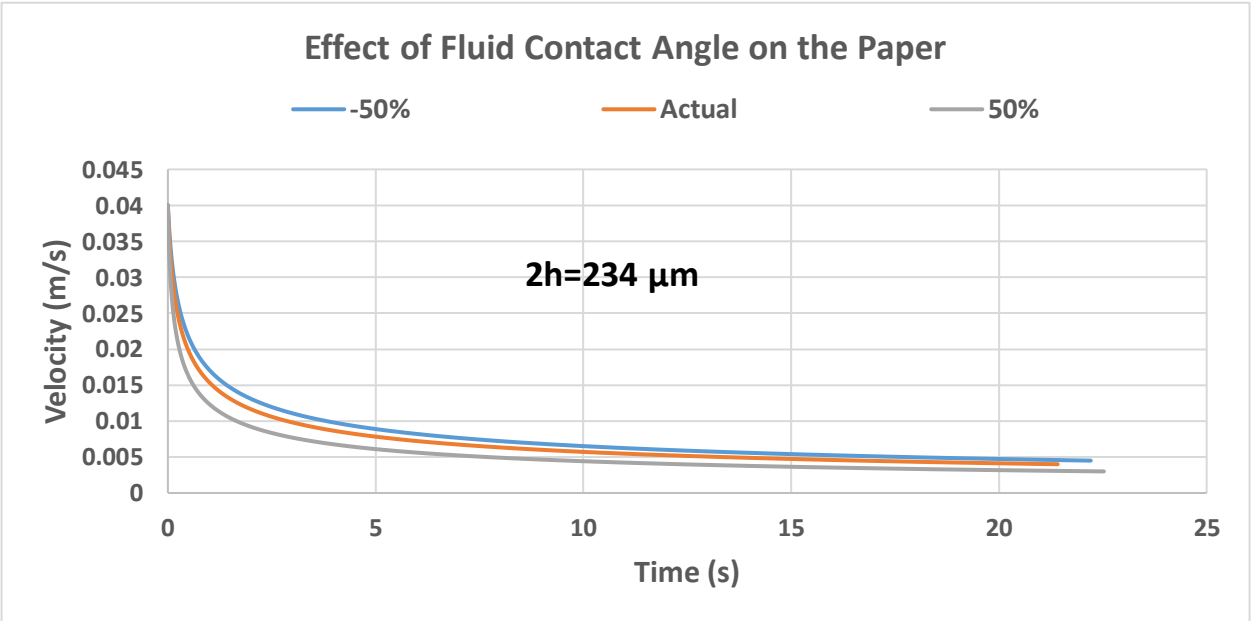

Figure 4.28: Velocity VS Time for 234 µm gap height with 03 different fluid contact angles on the paper

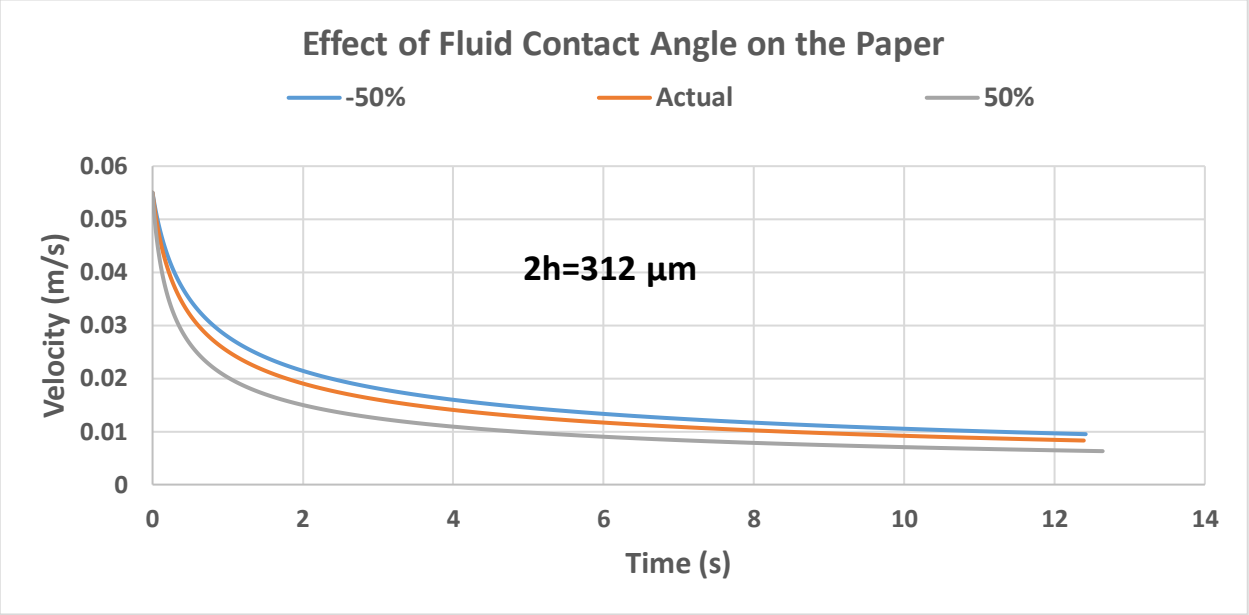

Figure 4.29: Velocity VS Time for 312 µm gap height with 03 different fluid contact angles on the paper

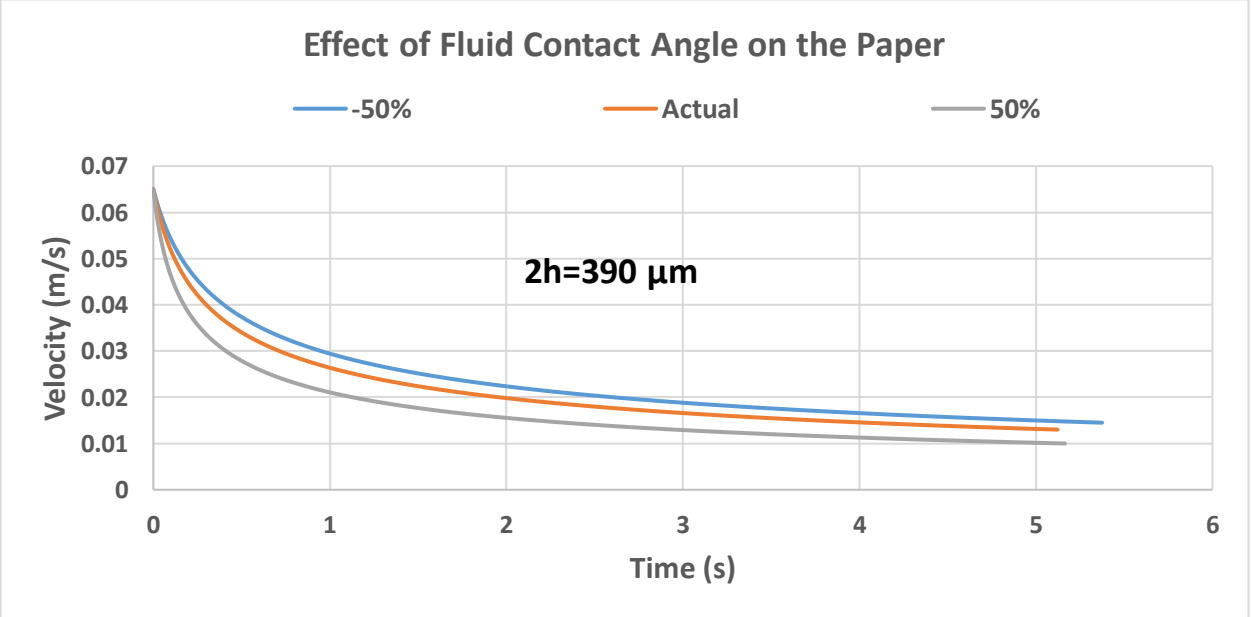

Figure 4.30: Velocity VS Time for 390 µm gap height with 03 different fluid contact angles on the paper

Fluid contact angle is found to be inversely proportional to velocity of fluid however according to Lucas Washburn equation [47,79] it is found directly proportional to penetration length but in this case it the angle of fluid in paper made with hydrophobic boundary which causes the fluid to behave inversely in relation to fluid velocity.

4.5.6 Effect of gap height:

Below figure shows the effect of different gap heights on velocity profile.

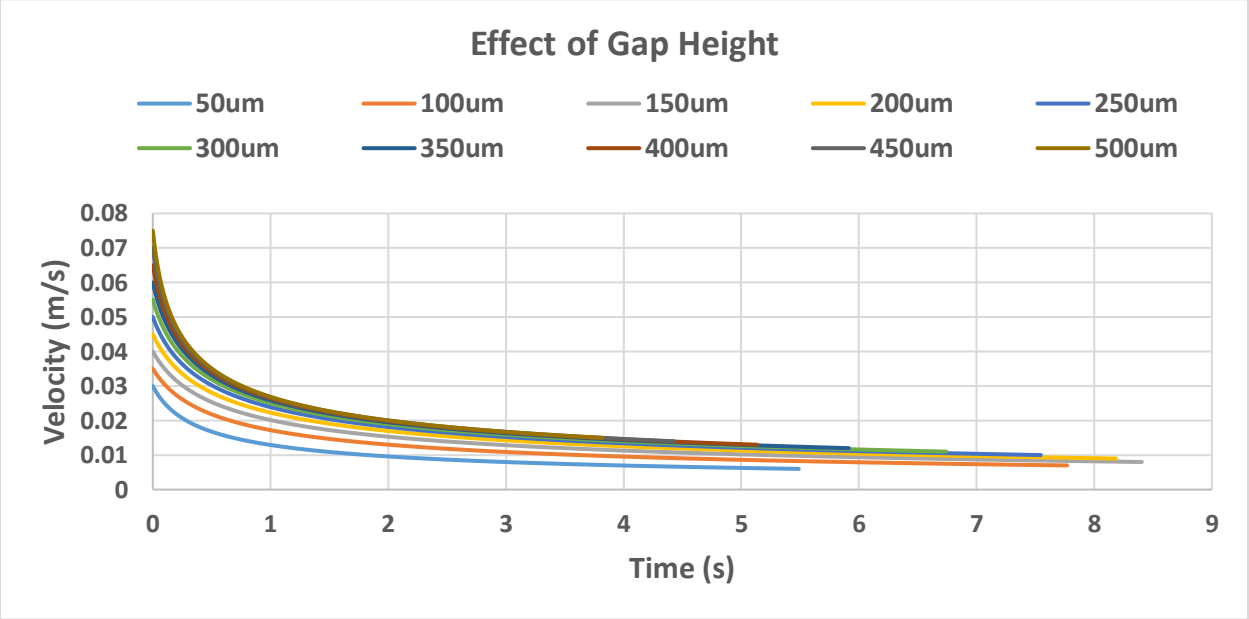

Figure 4.31: Velocity VS Time for 10 different gap heights

It is the sheer magnitude of the Laplace pressure driving force in the gap between the paper layers that the flow in the gap is dragging the liquid in the paper layer and the flow in that region is dominated by the “moving wall” of the liquid at the gap boundary.

5 : CONCLUSION AND FUTURE RECOMMENDATIONS

It is concluded that in case of single and multilayered µPADs, Whatman filter paper grade 4 is recommended because in this grade of paper material, fluid has taken minimum time to reach maximum height of 0.12m and fluid velocity through this grade is found to be 1.3 mm/s which is 92% enhanced as compared to filter paper grade 1, 83.85% enhanced as compared to filter paper grade 3, and 94.6% enhanced as compared to filter paper grade 5.

Pore radius is found to be directly proportional with the velocity of fluid; however porosity doesn't affect velocity value in case of single layered µPADs.

Optimum value of paper width is found to be 0.02m and it gives us maximum velocity enhancement and beyond that there is no considerable variation found in velocity.

Permeability, interfacial surface tension, paper thicknesses are found to be directly proportional to the velocity of fluid in case of numerical analysis on multilayered µPADs.

Fluid contact angle on paper and fluid dynamic viscosity are found to be inversely proportional to velocity of fluid. In multilayered µPADs, maximum gap height that is beneficial for fluid enhancement is 400 µm and beyond that there is no considerable effect on fluid velocity with the increase in gap height.

Based on these findings one can manufacture filter paper with certain desired properties to get desirable results in terms of velocity of fluid and can fabricate multilayered µPADs while considering gap height parameter.

Future recommendation includes:

- Theoretical modeling which accurately depicts behavior of fluid flow through multilayered (µPADs) considering all design parameters.
- To improve shelf life of reagents/enzymes stored on µPADs.
- To overcome Coffee Ring effect developed on paper material near hydrophobic boundary.
- Build a model on COMSOL Multiphysics to numerically analyze multilayered (µPADs).

- Perform multiple experiments using complex shaped Multilayered (µPADs) and observe behavior of all the design parameters involved in it.
- Make homogeneous paper material having isotropic properties.

REFRENCES

1. A. Ern, I. M. (2010). Discontinuous Galerkin approximation of two-phase flows in heterogeneous porous media with discontinuous capillary pressures. *Computer Methods in Applied Mechanics and Engineering*, 199,23-24,1491-1501.

2. A. Montillet, E. A. (2007). About a correlating equation for predicting pressure drops through packed beds of spheres in a large range of Reynolds numbers. *Chemical Engineering and Processing: Process Intensification*, 46,4,329-333.

3. Ali Al-Maktoumi, A. K.-I.-B.-S. (2015). Infiltration into Two-Layered Soil: The Green-Ampt and Averyanov Models Revisited. *Transport in Porous Media*, 109,169-193.

4. Ali K. Yetisen, J. L.-H.-M. (2014). A smartphone algorithm with inter-phone repeatability for the analysis of colorimetric tests. *Sensors and Actuators B: Chemical*, 196-156-160.

5. Amiri, M. R. (2017). Phase-field simulation of counter-current spontaneous imbibition in a fractured heterogeneous porous medium. *Physics of Fluids*, 29,6,062104.

6. Andres W. Martinez, S. T. (2007). Patterned Paper as a Platform for Inexpensive, Low-Volume, Portable Bioassays. *Angewandte Chemie*, 46,1318-1320.

7. Andres W. Martinez, S. T. (2008). FLASH: A rapid method for prototyping paper-based microfluidic devices. *Lab on a Chip*, 8,12,2146-2150.

8. Andres W. Martinez, S. T. (2008). Simple Telemedicine for Developing Regions: Camera Phones and Paper-Based Microfluidic Devices for Real-Time, Off-site Diagnosis. *Analytical Chemistry*, 80,10,3699-3707.

9. Andres W. Martinez, S. T. (2010). Diagnostics for the Developing World: Microfluidic Paper-Based Analytical Devices. *Analytical Chemistry*, 82,1,3-10.

10. Angel Perez-Cruz, I. S.-G. (2017). Two-dimensional model of imbibition into paper-based networks using Richards equation. *Microfluidics and Nanofluidics*, 21,5,98.

11. Audrey K. Ellerbee, S. T. (2009). Quantifying Colorimetric Assays in Paper-Based Microfluidic Devices by Measuring the Transmission of Light through Paper. *Analytical Chemistry*, 81,20,8447-8452.

12. B. Manori Jayawardane, I. D. (2012). A paper-based device for measurement of reactive phosphate in water. *Talanta*, 100,454-460.

13. Benjamin Dietrich, W. S. (2009). Pressure drop measurements of ceramic sponges-Determining the hydraulic diameter. *Chemical Engineering Science*, 64,16,3633-3640.

14. Bingbing Gao, J. C. (2017). Vertical Paper Analytical Devices Fabricated Using the Principles of Quilling and Kirigami. *Scientific Reports*, 7,7255.

15. BV Antohe, J. L. (1997). Experimental determination of permeability and inertia coefficients of mechanically compressed aluminium porous matrices. *Journal of Fluids Engineering*, 119,404-412.

16. Clegg, R. H. (1949). Automatic Paper Chromatography. *Analytical Chemistry*, 21,9,1123-1125.

17. Conor K. Camplisson, K. M. (2015). Tow-ply channels for faster wicking in paper-based microfluidic devices. *Lab on a Chip*, 15,23,4461-4466.

18. Darcy, H. (1856). *Les fontaines publiques de la ville de Dijon: exposition et application.* Victor Dalmont.

19. Derek A. Bruzewicz, M. R. (2008). Low-Cost Printing of Poly(dimethylsiloxane) Barriers To Define Microchannels in Paper. *Analytical Chemistry*, 80,9,3387-3392.

20. Dharitri Rath, N. S. (2018). Experimental Measurement of Parameters Governing Flow Rates and Partial Saturation in Paper-Based Microfluidic Devices. *Langmuir*, 34,30,8758-8766.

21. Dr. Jixian Yan, D. L. (2012). Paper-Based Electrochemiluminescent 3D Immunodevice for Lab-on-Paper, Specific, and Sensitive Point-of-Care Testing. *Chemistry A European Journal*, 18,16,4938-4945.

22. Durlofsky, L. J. (1991). Numerical calculation of equivalent grid block permeability tensors for heterogeneous porous media. *Water Resources Research* , 27,5,699-708.

23. Emanuel Elizalde, R. U. (2015). Rational design of capillary-driven flows for paper-based microfluidics. *Lab on a Chip*, 15,10,2173-2180.

24. Fan, K. W. (2015). Mixing in microfluidic devices and enhancement methods. *Journal of Micromechanics and Microengineering*, 25,094001.

25. Fan, X. J. (2016). Fabrication and Operation of Paper-Based Analytical Devices. *Annual Review of Analytical Chemistry*, 9,203-222.

26. Fernando J. Guerrero-Martinez, P. L. (2017). Three-dimensional numerical simulations of free convention in a layered porous enclosure. *International Journal of Heat and Mass Transfer*, 106,1005-1013.

27. *Filter Paper*. (n.d.). Retrieved from Indiamart: https://www.indiamart.com/proddetail/whatman-filter-paper-16686076597.html

28. GS Beavers, E. S. (1969). Non-Darcy flow through fibrous porous media. *Journal of Applied Mechanics*, 36,711-714.

29. GS Beavers, E. S. (1973). Influence of Bed size on the flow characteristics and porosity of randomly packed beds of spheres. *Applied Mechanics*, 40,655-660.

30. Helmig, R. (1997). *Multiphase flow and transport processes in the subsurface*. Berlin: Springer.

31. Hu Wang, Y.-j.-L. J.-f.-r.-h.-x. (2014). Paper-based three-dimensional microfluidic device for monitoring of heavy metals with a camera cell phone. *Analytical and Bioanalytical Chemistry*, 406,2799-2807.

32. Huinink, H. (2016). Fluids in Porous Media. In H. Huinink, *Fluids in Porous Media*.

33. II, N. D. (2011). A two-permeability approach for assessing flow properties in metal foam. *Journal of Porous Materials*, 18,417-424.

34. J. F. Liu, W. T. (2006). Measurement and correlation of friction chracteristic of flow through foam matrixes. *Experimental Thermal and Fluid Science*, 30,4,329-336.

35. J. Israel Martinez-Lopez, M. M. (2016). Xurography as a Rapid Fabrication Alternative for Point-of-Care Devices: Assessment of Passive Micromixers. *Sensors*, 16,5,705.

36. Jacob Bear, C. B. (1972). On the flow of two immiscible fluids in fractured porous media. *Developements in soil science*, 2,177-202.

37. JE Warren, H. P. (1961). Flow in heterogeneous porous media. *Society of Petroleum Engineers Journal*, 1,3,153-169.

38. Jianchao Cai, E. P.-L. (2014). Generalized Modeling of Spontaneous Imbibition Based on Hagen-Poiseuille Flow in Tortuous Capillaries with Variably Shaped Apertures. *Langmuir*, 30,18,5142-5151.

39. Junfeng Xiao, H. A. (2012). Source-like Solution for Radial Imbibition into a Homogeneous Semi-infinite Porous Medium. *Langmuir*, 28,9,4208-4212.

40. Junfeng Xiao, J. C. (2018). Saturated imbibition under the influence of gravity and geometry. *Journal of Colloid and Interface Science*, 521,226-231.

41. Kausik Bal, J. F. (2011). Differential spontaneous capillary flow through heterogeneous porous media. *International Journal of Heat and Mass transfer*, 54,13-14,3096-3099.

42. Ke Yang, H. P.-S. (2016). Novel developments in mobile sensing based on the integration of microfluidic devices and smartphones. *Lab on a Chip*, 16,6,943-958.

43. Klinkenberg, L. (1941). The permeability of porous media to liquids and gases. *American Petroleum Institute of Drilling and Production Practice*, 200-213.

44. Koji Abe, K. S. (2008). Inkjet-Printed Microfluidic Multianalyte Chemical Sensing Paper. *Analytical Chemistry*, 80,18,6928-6934.

45. L. Zhuang, S. M. (2017). Revisiting the horizontal redistribution of water in soils: Experiments and numerical modeling. *Water Resources Research*, 53,9,7576-7589.

46. Lei Ge, J. Y. (2012). Three-dimensional paper-based electrochemiluminescence immunodevice for multiplexed measurement of biomarkers and point-of-care testing. *Biomaterials*, 33,4,1024-1031.

47. Lucas, R. (1918). Ueber das Zeitgesetz des kapillaren Aufstiegs von Flussigkeiten. *Kolloid-Zeitschrift*, 23,1,15-22.

48. M. Le Bars, M. G. (2006). Interfacial conditions between a pure fluid and a porous medium: implications for binary alloy solidification. *Journal of Fluid Mechanics*, 550,149-173.

49. M. Mohammadifar, J. Z. (2018). Power-on-paper: Origami-inspired fabrication of 3-D microbial fuel cells. *Renewable Energy*, 118,695-700.

50. M. Monsur Ali, C. L.-A. (2017). A Printed Multicomponent Paper Sensor for Bacterial Detection. *Scientific Reports*, 7,12335.

51. M. Reyssat, L. Y. (2009). Imbibition in layered systems of packed beads. *Europhysics Letters*, 86,5,56002.

52. M. Schneider, T. K. (2018). Stable Propagation of Saturation Overshoots for Two-Phase Flow in Porous Media. *Transport in Porous Media*, 121,621-641.

53. Mallory M. Mentele, J. C. (2012). Microfluidic Paper-Based Analytical Device for Particulate Metals. *Analytical Chemistry*, 84,10,4474-4480.

54. Marina Cretich, V. S. (2010). Coating of nitrocellulose for colorimetric DNA microarrays. *Analytical Biochemistry*, 397,1,84-88.

55. Meher, H. S. (2017). Modelling of Imbibition Phenomena in Fluid Flow through Heterogeneous Inclined Porous Media with different porous materials. *Nonlinear Engineering*, 6,4,263-275.

56. *Merck*. (n.d.). Retrieved from sigmaaldrich: https://www.sigmaaldrich.com/PK/en/product/aldrich/wha1001325?lang=en&region=US&gclid=CjwKCAjw6raYBhB7EiwABge5KkIT8lw4KSnBH4gpXWGtdS6AK7MrfGSbICZfKcXMZSqSPGBHXIuE6hoCqtIQAvD_BwE

57. Michael A. A. Spaid, F. R. (1998). Modeling void formation dynamics in fibrous porous media with the lattice Boltzmann method. *Composites Part A: Applied Science and Manufacturing*, 29,7,749-755.

58. Michael Conrath, N. F. (2010). Radial Capillary Transport from an Infinite Reservoir. *Transport in Porous Media*, 84,1,109-132.

59. Mingchao Liu, J. W. (2016). Evaporation Limited Radial Capillary Penetration in Porous Media. *Langmuir*, 32,38,9899-9904.

60. Mingchao Liu, J. W. (2018). Tuning capillary penetration in porous media: Combining geometrical and evaporation effects. *International Journal of Heat and Mass Transfer*, 123,239-250.

61. N. Fries, K. O. (2008). The effect of evaporation on the wicking of liquids into a metallic weave. *Journal of Colloid and Interface Science*, 321,1,118-129.

62. N. Scott Lynn Jr., J.-I. M.-L. (2014). Biosensing enhancement using passive mixing structures for microarray-based sensors. *Biosensors and Bioelectronics*, 54,506-514.

63. Nihad Dukhan, P. P. (2008). Equivalent particle diameter and length scale for pressure drop in porous metals. *Experimental Thermal and Fluid Science*, 32,5,1059-1067.

64. Norman R Morrow, G. M. (2001). Recovery of oil by spontaneous imbibition. *Current Opinion in Colloid and Interface Science*, 6,4,321-337.

65. Onur Mudanyali, S. D. (2012). Integrated rapid-diagnostic-test reader platform on a cellphone. *Lab on a Chip*, 12,15,2678-2686.

66. Organization, W. H. (2011). Guidelines for Drinking-water Quality, Edition F. In W. H. Organization.

67. Pettersen, O. (1987). Simulation of two-phase flow in porous rocks on a laboratory scale: Diffusion operator splitting and consistency. *Computer Methods in Applied Mechanics and Engineering*, 65,3,229-252.

68. Poomrat Rattanarat, W. D. (2014). Multilayer Paper-Based Device for Colorimetric and Electrochemical Quantification of Metals. *Analytical Chemistry*, 86,7,3555-3562.

69. Quere, D. (1997). Inertial Capillarity. *EPL (Europhysics Letters)*, 39,5,533.

70. Rainer Helmig, A. W. (2007). Dynamic capillary effects in heterogeneous porous media. *Computational Geosciences*, 11,3,261-274.

71. Rasi, M. (2013). Permeability Properties of Paper Materials. In M. Rasi, *Permeability Properties of Paper Materials* (p. 59). Jyvaskyla, Finland.

72. Richard J. Block, E. L. (2016). *A Manual of Paper Chromatography and Paper Electrophoresis.* Elsevier.

73. Robert B. Channon, M. P. (2019). Multilayered Microfluidic Paper-Based Devices: Characterization, Modeling, and Perspectives. *Analytical Chemistry*, 8966-8972.

74. Ruihua Tang, H. Y. (2017). Improved Analytical Sensitivity of Lateral Flow Assay using Sponge for HBV Nucleic Acid Detection. *Scientific Reports*, 7,1,1360.

75. Seokbin Hong, a. W. (2015). Dynamics of water imbibition through paper channels with wax boundaries. *Microfluidics and Nanofluidics*, 19,4,845-853.

76. Sergio Mendez, E. M. (2009). Imbibition in Porous Membranes of Complex Shape: Quasi-stationary Flow in Thin Rectangular Segments. *Langmuir*, 26,2,1380-1385.

77. Shunxing Su, R. N. (2007). Adsorption and Covalent Coupling of ATP-Binding DNA Aptamers onto Cellulose. *Langmuir*, 23,3,1300-1302.

78. Thu H Nguyen, A. F. (2014). Paper-based batteries: A review. *Biosensors and Bioelectronics*, 54,640-649.

79. Washburn, E. W. (1921). The Dynamics of Capillary Flow. *Physical Review*, 17,3,273-283.

80. Weibo Li, D. Q. (2016). Fully-drawn origami paper analytical device for electrochemical detection of glucose. *Sensors and Actuators B: Chemical*, 231,230-238.

81. Wijitar Dungchai, O. C. (2009). Electrochemical detection for Paper-Based Microfluidics. *Analytical Chemistry*, 81,14,5821-5826.

82. Wijitar Dungchai, O. C. (2010). Use of multiple colorometric indicators for paper-based microfluidic devices. *Analytica Chimica Acta*, 674,2,227-233.

83. Win Loung Chiou, L. D. (1970). Adsorption of Organic Compounds by Commercial Filter Papers and its Implication on Quantitative-Qualitative Chemical Analysis. *Journal of Pharmaceutical Sciences*, 59,6,,843-847.

84. Xu Li, J. T. (2008). Paper-Based Microfluidic Devices by Plasma Treatment. *Analytical Chemsitry*, 80,23,9131-9134.

85. Yacine Debbabi, M. D. (2017). Viscous Crossflow in Layered Porous Media. *Transport in Porous Media*, 117,2,281-309.

86. Yao Lu, W. S. (2009). Rapid prototyping of paper-based microfluidics with wax for low cost, portable bioassay. *Electrophoresis*, 30,9,1497-1500.

87. Yi Jin, X. L. (2017). A mathematical model of fluid flow in tight porous media based on fractal assumptions. *International Journal of Heat and Mass Transfer*, 108,1078-1088.

88. Yu, J. C. (2011). A Discussion of the Effect of Tortuosity on the Capillary Imbibition in Porous Media. *Transport in Porous Media*, 89,251-263.

89. Zheng Kun-Can, W. T.-C.-J.-F. (2017). Fractal analysis of flow resistance in random porous media based on the staggered pore-throat model. *International Journal of Heat and Mass Transfer*, 115,225-231.

90. Zhi Liu, J. H. (2015). Experimental and numerical studies on liquid wicking into filter papers for paper-based diagnostics. *Applied Thermal Engineering*, 88,280-287.

91. Zhihong Nie, F. D. (2010). Integration of paper-based microfluidic devices with commercial electrochemical readers. *Lab on a Chip*, 10,22,3163-3169.